

Relativistic Density Functional Calculations of Hyperfine Coupling with Variational versus Perturbational Treatment of Spin–Orbit Coupling

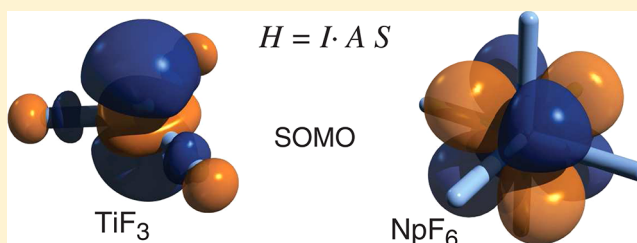
Prakash Verma and Jochen Autschbach*

Department of Chemistry, University at Buffalo, State University of New York, Buffalo, New York 14260-3000

S Supporting Information

ABSTRACT: Different approaches are compared for relativistic density functional theory (DFT) and Hartree–Fock (HF) calculations of electron–nucleus hyperfine coupling (HFC) in molecules with light atoms, in transition metal complexes, and in selected actinide halide complexes with a formal metal $5f^1$ configuration. The comparison includes hybrid density functionals with range-separated exchange. Within the variationally stable zeroth-order regular approximation (ZORA) relativistic framework, the HFC is obtained

(i) with a linear response (LR) method where spin–orbit (SO) coupling is treated as a linear perturbation, (ii) with a spin-polarized approach closely related to a DFT method for calculating magnetic anisotropy (MA) previously devised by van Wüllen et al. where SO coupling is included variationally, (iii) with a quasi-restricted variational SO method previously devised by van Lenthe, van der Avoird, and Wormer (LWA). The MA and LWA approaches for HFC calculations were implemented in the open-source NWChem quantum chemistry package as part of this study. The methodology extends recent implementations for calculations of electronic g -factors (*J. Chem. Theor. Comput.* **2013**, *9*, 1052). The impact of electron correlation (DFT vs HF) and DFT delocalization errors, the effects of spin-polarization, the importance of treating spin–orbit coupling beyond first-order, and the magnitude of finite-nucleus effects, are investigated. Similar to calculations of g -factors, the MA approach in conjunction with hybrid functionals performs reasonably well for theoretical predictions of HFC in a wide range of scenarios.



1. INTRODUCTION

The interaction of electromagnetic fields with electric and magnetic moments of molecules can be calculated using a variety of quantum chemical methods. The same interactions can be probed experimentally with a plethora of techniques, thus yielding important information about the electronic structure and bonding in molecules. Quantum chemical methods are vital for developing a deep understanding of the dominant factors leading to a particular measured value.

This work is concerned with certain aspects of the intramolecular interactions between electron spins and nuclear spins in systems with unpaired electrons giving rise to the electron–nucleus hyperfine coupling (HFC). Hyperfine coupling can be observed in electron paramagnetic resonance (EPR) experiments¹ as well as other types of spectroscopy. Interactions between electron and nuclear spins are also key to the understanding of NMR chemical shifts in paramagnetic molecules.^{2,3} In both contexts, phenomenological spin Hamiltonians are used to describe the magnetic interactions of quantized electronic (pseudo-) spins with external and internal electromagnetic fields. For HFC, the EPR spin Hamiltonian for a nucleus N can be written as

$$H = \mathbf{I}_N \cdot \mathbf{A}_N \mathbf{S} \quad (1)$$

where \mathbf{S} is the effective spin operator of the electronic system (components S_x , S_y , S_z), and \mathbf{I}_N is the nuclear spin vector. A

hyperfine magnetic field is associated with the nuclear magnetic moment $\mathbf{m}_N = g_N \beta_N \mathbf{I}_N$, which is treated semiclassically here. In the definition of \mathbf{m}_N , g_N is the nuclear g -factor, and β_N is the nuclear magneton. The 3×3 matrix \mathbf{A}_N in eq 1 describes the hyperfine coupling. We shall refer to \mathbf{A}_N as the HFC matrix. The hyperfine coupling constant is denoted by A_N . Similar to its counterpart in EPR spectroscopy, the so-called g -‘tensor’ (more properly termed the Zeeman coupling matrix¹), \mathbf{A}_N is not a tensor.⁴ A hyperfine coupling related to a selected quantization direction \mathbf{q} , for example, as defined by the external magnetic field direction of the EPR spectrometer or some symmetry axis in a molecule, can be defined similar to a principal g -factor via

$$|A_N| = (\mathbf{q} \cdot \mathbf{A}_N \mathbf{A}_N^T \mathbf{q})^{1/2} \quad (2)$$

(superscript T indicates a matrix transpose, and \mathbf{q} is assumed to be normalized). The quantity $\mathbf{A}_N \mathbf{A}_N^T$ is a rank-2 tensor. Its eigenvectors define a principal axis system (PAS) for hyperfine coupling, and its eigenvalues correspond to the squares of the principal HFC values.

Hyperfine coupling has been of interest since the early days of modern quantum theory^{5–13} for a number of reasons, among

Received: December 20, 2012

Published: February 12, 2013

which are (i) it is observed in atomic spectroscopy with high accuracy, (ii) it is very sensitive to the electronic structure, and (iii) HFC may afford large relativistic effects and significant finite nucleus effects. Therefore, HFC provides a great testing ground for quantum theoretical methods. HFC has a nonvanishing nonrelativistic limit. Computations at this theoretical level have been performed for a long time with a variety of quantum chemical approaches.¹⁴ Generally applicable relativistic quantum chemistry approaches for molecules have reached a mature level.^{15–18} Corresponding methods for HFC been put forward (selected references are provided below). Relativistic effects on HFC may well exceed the magnitude of a nonrelativistic result for a nucleus of an element of the sixth row of the periodic table (e.g., Hg) or beyond. Even finite-nucleus corrections were shown to be on the order of -10% to -15% relative to relativistic point-nucleus calculations for radicals containing Hg, and were correspondingly larger for nuclei with higher charge.^{19,20,50,66} These effects are mostly of the scalar relativistic type, which lead to a strong increase of the electron density and spin magnetization around a heavy nucleus. Spin–orbit (SO) coupling is another relativistic effect arising from magnetic interactions of the electron orbital motion and the electron spin that vanish in the nonrelativistic limit. In systems with very heavy elements such as actinides, SO coupling has the potential to qualitatively alter the bonds around the heavy element, which may therefore have a strong impact on HFC of ligands bound to a paramagnetic metal center. Furthermore, the effects of SO coupling on a heavy atom HFC may be substantial. For all the above reasons, a proper theoretical description of HFC for molecules with elements from across the periodic table requires a relativistic quantum theoretical framework.^{16,18,21,22}

A hierarchy of approximations can be devised for molecular quantum chemical calculations of HFC, based on the level at which electron correlation, scalar relativistic effects, spin–orbit coupling, spin-polarization effects, and operators that contribute to HFC, are treated. As already mentioned, HFC has a nonvanishing nonrelativistic limit, and therefore, it has been studied very extensively with nonrelativistic methods for molecules with light atoms¹⁴ such as organic radicals, as well as for light transition metals and for ligands in their complexes.^{23,24} In the simplest case, one neglects correlation and relativistic effects and obtains HFC constants with semiempirical molecular orbital models,^{25–28} or with Hartree–Fock (HF) theory and its semiempirical approximations in spin-unrestricted form²⁹ or with projection techniques to eliminate contaminating spin states.³⁰ A comparison of different spin-polarized models (spin-unrestricted approaches, both without and with removal of spin contamination) with spin-restricted treatments, has been made in ref 31. Electron correlation can be included in many ways such as by many-body perturbation theory (MBPT),^{32–34} configuration interaction (CI),^{35–42} coupled-cluster (CC) theory,^{32,43} and symmetry adapted cluster methods (SAC).^{44,45} A study of the influence of various excitation classes in CI to obtain accurate spin-densities can be found in an article by Engels.⁴⁶ Obtaining molecular properties with wave function methods such as MBPT and truncated CC requires recasting the energy functionals to account for the fact that the energies are not variational in these methods.^{43,47} Less preferred are finite field methods, which, however, can deliver accurate results without the need to develop analytic nonvariational derivative techniques.³² By ignoring correlation but including relativistic

effects, HF theory can be used to calculate HFC constants in systems with heavy elements.⁴⁸ Using a four-component relativistic Hamiltonian together with many-body correlation methods, one can obtain hyperfine coupling constants very accurately.^{49–54} However, due to their high computational cost such calculations have been tested mostly on atomic systems. A spin-free two-component relativistic approach has recently been used for correlated wave function-based calculations of HFC constants in radicals containing mercury.⁵⁵

Electron correlation can alternatively be treated within the framework of density functional theory (DFT). We focus here on Kohn–Sham (KS) DFT. In a nonrelativistic or relativistic DFT framework, HFC can be calculated at a manageable computational cost. In principle, DFT provides an effective solution of the correlation problem. In practice, the performance of approximate functionals requires careful testing for a particular intended purpose. Furthermore, new developments may lead to well-performing relativistic functionals^{56,57} although a significant improvement over nonrelativistic functionals for molecular observables is yet to be demonstrated.⁵⁸ There is also the problem of treating open-shell heavy atom systems with pronounced multireference character in the Kohn–Sham framework with approximate functionals. These issues affect DFT calculations of many types of spectroscopic parameters, including EPR. The Slater exchange functional and uncoupled KS perturbation theory has been used in some of the early DFT work to obtain hyperfine coupling constants.⁵⁹ For early work using local density approximation (LDA) and generalized gradient approximation (GGA) spin-density functionals; see, for example, refs 23, 60–64. Scalar relativistic effects can be included variationally into the KS Hamiltonian, for instance by using the Douglas–Kroll–Hess (DKH) operator⁶⁵ or the zeroth-order regular approximation (ZORA).⁶⁶ In such a framework, SO effects on HFC can be obtained by solving coupled KS equations in which SO coupling is one of the perturbations. For systems where SO coupling is strong, scalar and SO effects can both be incorporated variationally into the KS Hamiltonian, either at a 2-component⁶⁷ or at a 4-component KS level.⁶⁸

In a recent article,⁶⁹ herein referred to as Paper I, we made a side-by-side comparison of different conceptual approaches by which EPR *g*-factors (or *g*-shifts, i.e., deviations from the free-electron *g*-value) can be obtained from variational relativistic DFT and HF calculations in which SO coupling was either included variationally or treated as a perturbation. For earlier related studies of *g*-shifts see refs 70 and 71. A main concern in Paper I has been the performance of various classes of density functionals, namely functionals with local DFT exchange, global hybrids with a constant fraction of nonlocal exact exchange, and hybrids with range-separated exchange. It was found that with increasing nuclear charge, factors influencing the *g*-tensor, viz. perturbational vs variational inclusion of SO coupling, inclusion or exclusion of spin-polarization, and the treatment of correlation and exchange, may show a complex interdependence. Hybrid functionals in conjunction with a variational treatment of SO coupling were found to perform reasonably well.

The present work is concerned with a similar comparison for HFC. The ZORA relativistic framework is applied to a benchmark set comprised of molecules and complexes with main group atoms, light and heavy transition metals, and actinides. For consistency, the same basis sets, functionals, and integration grids are employed for different types of HFC

calculations on a given system. All calculations were performed with the open-source NWChem package.⁷² The HFC calculations differ in the way that SO coupling and spin-polarization are treated. Comparison is made among (i) Linear response (LR) calculations where SO coupling is not included in the ground state electronic structure but treated as a linear perturbation (a LR ZORA implementation for HFC in NWChem used for these calculations was recently reported by us.⁶⁶); (ii) a Kramers-doublet method devised by van Lenthe, Wormer, and Avoird (LWA)⁶⁷ where SO coupling is treated variationally in a quasi-restricted setup (a ZORA implementation of the LWA hyperfine coupling formalism in NWChem is reported herein.); and (iii) variational calculations including SO coupling, with different orientations of the spin-quantization axis. The latter method is inspired by, and closely related to, recent work by van Wüllen et al. on the calculating zero-field splitting and magnetic anisotropy (MA)^{73,74} and therefore herein referred to as the MA approach. Functionality for the required generalized-collinear SO DFT ZORA calculations was implemented in NWChem for Paper I. The program module's functionality has been extended for the present work to enable HFC calculations.

In Section 2, theoretical details regarding the LR, LWA, and MA calculations of HFC with ZORA-DFT are briefly summarized. Computational details are provided in Section 3. Results obtained for a benchmark set of molecules and metal complexes with light to heavy atoms are discussed in Section 4. Concluding remarks can be found in Section 5.

2. THEORY

The formalism closely follows that for EPR g -factors implemented in the NWChem code (see Paper I⁶⁹ and previous LR implementations of g -factors and hyperfine coupling with ZORA in the same program^{66,75}) and is therefore only summarized briefly to illustrate the methodology. Hartree atomic units with $e = 1$, $m_e = 1$, $\hbar = 1$, $4\pi\epsilon_0 = 1$, $c = \alpha^{-1} \approx 137.036$, $\mu_0/4\pi = c^{-2}$ are used unless explicitly noted otherwise.

2.1. Two-Component DFT Calculations. In the DFT and HF calculations with SO coupling included variationally, the 2-component KS Fock operator is $F = h + V_C + V_{XC}$. The operator h is the one-electron part of F , V_C is the electronic Coulomb potential, and V_{XC} is the exchange-correlation (XC) potential, the nonlocal exact exchange in HF theory, or a hybrid thereof. The field-free ZORA one-electron operator $h^{(0)}$ reads

$$h^{(0)} = V_{\text{ext}} + \frac{1}{2}(\boldsymbol{\sigma} \cdot \mathbf{p})\mathcal{K}(\boldsymbol{\sigma} \cdot \mathbf{p}) \quad (3)$$

where V_{ext} describes the interaction of the electron with the external potential from the atomic nuclei, $\boldsymbol{\sigma}$ is the 3-vector of the 2×2 Pauli spin matrices, $\mathbf{p} = -i\nabla$ is the linear momentum operator, and

$$\mathcal{K} = \frac{2c^2}{2c^2 - V} \quad (4)$$

In this work, the DFT component of V_{XC} is based on a nonrelativistic XC spin-density functional that is evaluated with the relativistic density and a suitably defined spin magnetization. The potential V in 4 is in principle the same as the SCF potential $V_{\text{ext}} + V_C + V_{XC}$. In the code, it is approximated as V_{ext} plus a sum of atomic electronic Coulomb potentials,⁷⁶ which is also used as an initial guess for the SCF step. The computations are performed either in spin-polarized form with an odd

number of singly occupied one- or two-component orbitals, or in the form of quasi-restricted KS calculations. The latter method produces orbitals that come in degenerate pairs, by assigning equal fractional occupations to a formally unpaired orbital (the 'singly occupied MO', or SOMO) and its degenerate counterpart. This quasi-restricted setup is used for the LWA-type calculations of HFC described in Section 2.3.

In the LR calculations of the HFC matrix, SO coupling is treated as a perturbation. A spin-unrestricted SCF calculation is in this case performed with the field-free scalar ZORA operator,

$$h_{\text{SC}}^{(0)} = V_{\text{ext}} + \frac{1}{2}\mathbf{p}\mathcal{K}\mathbf{p} \quad (5)$$

A 'spin-derivative' of the SO operator

$$h_{\text{SO}} = \frac{i}{2}\boldsymbol{\sigma} \cdot (\mathbf{p}\mathcal{K} \times \mathbf{p}) \quad (6)$$

is used in conjunction with the hyperfine operator (see below) for a double-perturbation (linear response, LR) calculation of the HFC matrix. We refer the reader to refs 66 and 77 for further details on ZORA-based LR implementations of hyperfine coupling.

2.2. Perturbation Operators. The nuclear magnetic vector potential for a selected nucleus N reads for a point-nucleus

$$\mathbf{A}_N = \frac{1}{c^2} \frac{\mathbf{m}_N \times \mathbf{r}_N}{r_N^3} \quad (7)$$

where \mathbf{r}_N is the distance vector from the nucleus, r_N its length, and \mathbf{m}_N is the nuclear spin magnetic moment. The factor of c^{-2} results from a conversion of $\mu_0/(4\pi)$ from the SI to atomic units. Minimal substitution $\mathbf{p} \rightarrow \mathbf{p} + \mathbf{A}_N$ in eq 3 or, alternatively, in the Dirac Hamiltonian before transformation to two-component form within the ZORA approximation,⁷⁸ gives the ZORA nuclear–electron hyperfine interaction operator

$$h^N = \frac{1}{2c^2} \left[\left(\frac{\mathbf{r}_N}{r_N^3} \times \mathbf{p} \right) \cdot \mathcal{K} \mathbf{m}_N + \mathcal{K} \mathbf{m}_N \cdot \left(\frac{\mathbf{r}_N}{r_N^3} \mathbf{p} \right) \right] + \frac{1}{2c^2} \boldsymbol{\sigma} \cdot \left\{ \mathbf{m}_N \left(\nabla \cdot \frac{\mathcal{K} \mathbf{r}_N}{r_N^3} \right) - (\mathbf{m}_N \cdot \nabla) \frac{\mathcal{K} \mathbf{r}_N}{r_N^3} \right\} \quad (8)$$

In eq 8, operators enclosed in curly brackets, $\{\dots\}$, indicate that derivatives are only taken inside the operator, not of functions that the operator is acting upon. The electron spin-independent part of eq 8 represents the ZORA analog of the nonrelativistic paramagnetic spin–orbital (PSO) term (sometimes labeled OP for 'orbital paramagnetic'). The electron-spin dependent operator (containing $\boldsymbol{\sigma}$) represents the sum of the ZORA analogs of the nonrelativistic Fermi-contact (FC) and spin-dipole (SD) terms. We use the same terminology here for the 2-component relativistic analogs. The nonrelativistic limit is formally obtained from eq 8 by letting $\mathcal{K} \rightarrow 1$ and subsequently taking the derivatives of \mathbf{r}_N/r_N^3 in the spin-dependent terms. For calculations of hyperfine perturbations, the derivative

$$\begin{aligned}
 h_u^N &= \frac{\partial h^N}{\partial m_{N,u}} \\
 &= \frac{1}{2c^2} \left[\left(\frac{\mathbf{r}_N}{r_N^3} \times [\mathbf{p}\mathcal{K} + \mathcal{K}\mathbf{p}] \right)_u \right. \\
 &\quad \left. + \left\{ \sigma_u \nabla \cdot \mathcal{K} \frac{\mathbf{r}_N}{r_N^3} - \sigma \cdot \nabla_u \mathcal{K} \frac{\mathbf{r}_N}{r_N^3} \right\} \right] \quad (9)
 \end{aligned}$$

is used, with subscript u indicating the x , y , or z component of a vector. For the HFC calculations, one needs

$$\frac{\partial h^N}{\partial I_{N,u}} = g_N \beta_N h_u^N \quad (10)$$

In the numerical quadrature used to obtain matrix elements of h_u^N , partial integration is used to avoid evaluating derivatives of \mathcal{K} and \mathbf{r}_N/r_N^3 by shifting the derivatives to the basis functions instead. Matrix elements in the AO basis are evaluated numerically using the same grids that are used for $h^{(0)}$ and the XC potential. For further details, see ref 66.

For heavy elements, HFC is sensitive to finite nuclear volume effects which arise from modifications of the ground state electron distribution as well as from modifications in the hyperfine perturbation operator (eq 9). The NWChem code supports ground state SCF calculations with a spherical Gaussian nuclear model.^{79,80} The hyperfine perturbation operator needs to be modified accordingly. The nuclear Gaussian exponent ξ_N can be obtained from $\xi_N = 3/(2R_N^2)$ where $R_N = (0.863M_N^{1/3} + 0.571) \text{ fm}$ is the RMS nuclear radius and M_N the mass number of the nucleus.⁷⁹ The effects from the finite nuclear volume are then incorporated in the perturbation operator (eq 9) by replacing $r_N^{-3}\mathbf{r}_N$ with $P(3/2, \xi_N r_N^2) r_N^{-3}\mathbf{r}_N$. Here, P is the lower incomplete gamma function ratio $P(q,r) = (1/\Gamma(q)) \int_0^r t^{q-1} e^{-t} dt$. Code for the calculation of $P(q,r)$ has been adapted from the scalar relativistic HFC implementation reported in ref 66. For further details, please see refs 81 and 66 and the articles cited therein. This approach does not consider details of how the nuclear magnetization density is distributed inside the nucleus relative to its charge density. Instead, the magnetization density is spread over a finite volume using the same Gaussian smearing as is used for the nuclear charge. The model is expected to capture the bulk of the finite nuclear volume effects. Finer details are likely to be negligible when considering the practically attainable accuracy of the electronic structure models in relativistic molecular computations.

2.3. Implementation Strategy for Hyperfine Coupling Using the LWA Approach. The approach follows the paper by van Lenthe, Wormer, and van der Avoird (LWA)⁶⁷ who adapted a strategy for two-component relativistic calculations of g -factors of Kramers doublets devised by the same authors⁸² for HFC. The Fock operator up to first order in the nuclear magnetic moment perturbation \mathbf{m}_N is expressed in the basis of one of the SOMO orbitals of a quasi-restricted calculation and its Kramers conjugate, with scalar and SO relativistic effects included variationally in the ground state calculation. The expression is interpreted as a matrix representation of the EPR spin-Hamiltonian in eq 1. The HFC matrix \mathbb{A} is then extracted directly from derivatives of the Hamiltonian matrix elements with respect to $I_{N,u}$. One of the orbitals with half occupancy from a quasi-restricted calculation is the designated SOMO and one member, Φ_1 , of a Kramers pair of orbitals. Its Kramers

conjugate Φ_2 is obtained by applying the one-electron time-reversal operator, $\Phi_2 = -i\sigma_y K_0 \Phi_1$. Here, K_0 is an antilinear operator that converts an orbital into its complex conjugate.²¹

The matrix elements of the Fock operator including the hyperfine perturbation are calculated in the basis $\{\Phi_1, \Phi_2\}$. Elements of the matrix \mathbb{A} are then obtained for the Kramers doublet ($S = 1/2$) as

$$\begin{aligned}
 A_{ux} &= \frac{g_N \beta_N}{S} \text{Re} \langle \Phi_1 | h_u^N | \Phi_2 \rangle = \frac{g_N \beta_N}{S} \text{Re} \langle \Phi_2 | h_u^N | \Phi_1 \rangle \\
 A_{uy} &= -\frac{g_N \beta_N}{S} \text{Im} \langle \Phi_1 | h_u^N | \Phi_2 \rangle = \frac{g_N \beta_N}{S} \text{Im} \langle \Phi_2 | h_u^N | \Phi_1 \rangle \\
 A_{uz} &= \frac{g_N \beta_N}{S} \text{Re} \langle \Phi_1 | h_u^N | \Phi_1 \rangle = -\frac{g_N \beta_N}{S} \text{Re} \langle \Phi_2 | h_u^N | \Phi_2 \rangle \quad (11)
 \end{aligned}$$

The derivation assumes that the KS orbitals minimize the energy functional. The operator h_u^N enters the expression from a derivative of the matrix elements with respect to $I_{N,u}$. It is assumed that the basis set is not dependent on the derivative parameter.

2.4. Implementation Strategy for Hyperfine Coupling Using the MA Approach. A row of the HFC matrix \mathbb{A} can alternatively be obtained via a DFT approach recently devised by van Wüllen et al. for calculations of zero-field splitting (ZFS) and magnetic anisotropy (MA).^{73,74} We refer to HFC within this framework as the MA approach. See Paper I and ref 83 for an equivalent technique to calculate electronic g -factors, and refs 73, 74, and 83 for additional details. The setup may be illustrated as follows: The expectation value of the EPR spin-Hamiltonian (1) for spin-1/2 taken with a Kohn–Sham determinant calculated with a spin-quantization axis \mathbf{q} reads

$$\begin{aligned}
 E(\mathbf{q}, I_N) &= \sum_i n_i \langle \varphi_i^q | \mathbf{I}_N \cdot \mathbb{A} \mathbf{S} | \varphi_i^q \rangle \\
 &= \sum_{uv} A_{uv} I_{N,u} \sum_i n_i \langle \varphi_i^q | S_v | \varphi_i^q \rangle \quad (12)
 \end{aligned}$$

with $u, v \in \{x, y, z\}$. For convenience, \mathbf{q} is assumed to be a normalized vector. In the previous equation, the φ_i^q are two-component KS orbitals obtained from a generalized collinear relativistic DFT calculation with selected spin-quantization axis \mathbf{q} , and the n_i are the occupation numbers. With pure spin-eigenfunctions, that is, in the absence of SO coupling, one finds

$$\sum_i n_i \langle \varphi_i^q | \mathbf{q} \cdot \mathbf{S} | \varphi_i^q \rangle = S = (n_\alpha - n_\beta)/2 \quad (13)$$

Here, n_γ is the sum of occupations of orbitals with positive ($\gamma = \alpha$) or negative ($\gamma = \beta$) projection along the chosen quantization axis. Let \mathbf{q} be parallel to a coordinate axis in direction v . The derivative of the right-hand side of eq 12 with respect to a component $I_{N,u}$ of the nuclear magnetic spin vector gives, with eq 13,

$$\frac{\partial E(v, I_N)}{\partial I_{N,u}} = S A_{uv} \quad (14)$$

In a generalized-collinear calculation with SO coupling included variationally, the $E(v, 0)$ may be different for different v because of magnetic anisotropy (which has been used by van Wüllen and co-workers⁷⁴ to extract the ZFS tensor from a set of calculations with different v). From the DFT energy expression, one obtains to first order in the nuclear spin

$$\frac{\partial E(v, I_N)}{\partial I_{N,u}} = \sum_i n_i \frac{\partial}{\partial I_{N,u}} \langle \varphi_i^v | F | \varphi_i^v \rangle \quad (15)$$

where the Fock operator is dependent on the nuclear spin. It follows from comparison of eq 14 with eq 15

$$A_{uv} = \frac{g_N \beta_N}{S} \sum_i n_i \langle \varphi_i^v | h_u^N | \varphi_i^v \rangle \quad (16)$$

where the operator h_u^N is given in eq 9. The basis set is assumed to be independent of the nuclear spin magnetic moment. The setup is based on three converged collinear SCF steps with SO coupling included variationally. Tight convergence is required in each of these steps in order to obtain well converged results. The calculations are facilitated by first performing a spin-unrestricted scalar relativistic calculation with z as the spin-quantization axis, and then restarting after rotating the spin-quantization direction for the converged scalar MOs for $v = x, y$. In the code, there is also the option to apply a small static external magnetic field in a given direction in order to align the electronic magnetic moments.

In the absence of SO coupling, the result simply amounts to the expectation value of $g_N \beta_N S^{-1} h_u^N$, where only the electron-spin dependent part (FC + SD) of h_u^N contributes because the PSO operator is imaginary. In relativistic calculations, the FC + SD term samples the electron spin density in the very vicinity of the nucleus,^{18,78} and scalar relativistic effects on HFC may be very large for heavy elements. In the LR calculations, there is a second term involving the PSO operator and the spin derivative of the SO operator. For the nonrelativistic limit $c \rightarrow \infty$, $\mathcal{K} \rightarrow 1$, this term vanishes because the SO operator vanishes. The LR and MA approaches then produce the same nonrelativistic result. With a finite speed of light, the MA approach incorporates linear as well as higher order SO effects. In the nonrelativistic limit, after taking the derivative of r_N/r_N^3 in the spin-dependent part of the operator h_u^N and assuming a point nucleus, the well-known expression for the Fermi contact term with its δ -distribution, and the nonrelativistic version of the dipolar term, are obtained. The isotropic HFC then samples the spin density right at the chosen point nucleus.

3. COMPUTATIONAL DETAILS

The molecule test set is comprised of three subsets. Subset I contains radicals with light main group elements: CH₃, HCO, HSiO, HSiS, SiOH, and SiSH. Subset II contains doublet radicals with light and heavy transition metals: TiF₃, TcNCl₄[−], ReNCl₄[−], HgH, HgF, HgCN, and HgAg. Subset III contains actinide elements in a formal $5f^1$ electronic configuration: NpF₆, UF₆[−], and UCl₆[−].

All computations were performed using a locally modified version of NWChem.⁸⁴ With the exception of HgCN and HgAg added here, the molecule test set is the same as in our recent study of g -factors calculated with LR, LWA, and MA approaches (Paper I). The basis sets and functionals used for the calculations are also comparable in most calculations. For C, H, N, O, F, Si, S, and Cl, the IGLO-III⁸⁵ basis was used. An uncontracted ANO-RCC basis^{86,87} was used for Ti, Hg, Tc, Re, U, and Np. g functions were removed from the Hg basis, and h functions were removed from the Ti, Np, and U basis sets. The following density functionals were employed: The Becke-88 exchange + Perdew-86 correlation (BP)^{88,89} and the Perdew–Burke–Ernzerhof (PBE)⁹⁰ nonhybrid functionals, a global hybrid version of PBE with 25% nonlocal exact exchange

(PBE0),⁹¹ a ‘coulomb attenuated’ range-separated hybrid functional with 19% nonlocal exact exchange at short interelectronic separations and 65% asymptotically (CAM-B3LYP, or short CAM),⁹² and a long-range (LR) corrected range-separated hybrid based on PBE0 with 25% nonlocal exact exchange at short interelectronic separations and 100% asymptotically (LC-PBE0). Additional calculations were carried out at the HF level.

Calculations with finite nuclear volumes employed a spherical Gaussian nuclear charge distribution with nuclear RMS radii calculated from the atomic mass as detailed in ref 79. ZORA perturbation operators for finite nuclei were employed as detailed in Section 2 (see also refs 66 and 81). In the comparison of finite vs point nucleus calculations, basis sets optimized for relativistic finite nucleus⁹³ (FN) and point nucleus⁹⁴ (PN) calculations were adopted in a fully uncontracted fashion and augmented with additional functions for the heavy atoms and polarization functions (from IGLO-III) for light atoms as suggested in refs 19 and 68.

The isotropic hyperfine coupling constants and principal components in units of MHz were obtained for the following nuclear isotopes (g_N values in parentheses): ¹H (5.5857), ¹³C (1.4048), ¹⁴N (0.40376), ¹⁷O (−0.7575), ¹⁹F (5.25773), ²⁹Si (−1.11057), ³³S (0.42921), ³⁵Cl (0.54791), ⁴⁷Ti (−0.31539), ⁹⁹Tc (1.2632), ¹⁰⁷Ag (−0.22714), ¹⁸⁷Re (1.2878), ¹⁹⁹Hg (1.01177), ²³⁵U (−0.1), ²³⁷Np (1.2560).

Optimized geometries for CH₃, HCO, HSiO, HSiS, SiOH, SiSH, HgH, HgF, TiF₃, HgCN, HgAg were taken from ref 75 (optimized with ADF⁹⁵ with scalar ZORA, the BP functional,^{88,89} and a triple- ζ doubly polarized (TZ2P) Slater-type basis). CASPT2 geometries for NpF₆, UF₆[−], and UCl₆[−] were taken from ref 96. Experimental geometries for the complexes TcNCl₄[−] and ReNCl₄[−] were taken from refs 97 and 98, respectively.

In the LR calculations, the HFC matrix is calculated and the symmetric part is diagonalized. The signs of the HFC components are reported as calculated. For the LWA and MA calculations, the matrix $\mathbb{A}\mathbb{A}^T$ of eq 2 is formed, and the HFC principal values A_{ii} , $i = 1 - 3$, are obtained as the square roots of the eigenvalues. The principal axis system (PAS) is given by the eigenvectors. Signs have been adjusted, where needed, to either match the LR results or by ensuring that the sign of the determinant of the HFC matrix before and after rotation to the PAS remains the same. The ordering adopted in some of the data tables is for the principal components, ordered as $A_{11} \leq A_{22} \leq A_{33}$. The isotropic HFC is given as $A_{\text{iso}} = (1/3) \sum_i A_{ii}$. For molecules with axial symmetry, we report the HFC values parallel (A_{\parallel}) and perpendicular (A_{\perp}) to the principal symmetry axis.

4. RESULTS AND DISCUSSION

4.1. Preliminary Considerations. For set I (light atoms), the choice between point nuclei (PN) and the finite nuclear (FN) model is irrelevant as both provide practically identical HFC constants (Table S1 in the Supporting Information (SI)). For Set I, we have used point nuclei, and for the heavier systems of Sets II and III, we have used a finite nuclear model consistently. Additional point-nucleus data are provided in the SI. A comparison between FN and PN is made for the Hg containing radicals in Section 4.4. Recent 4-component relativistic data obtained with the BP functional, and results

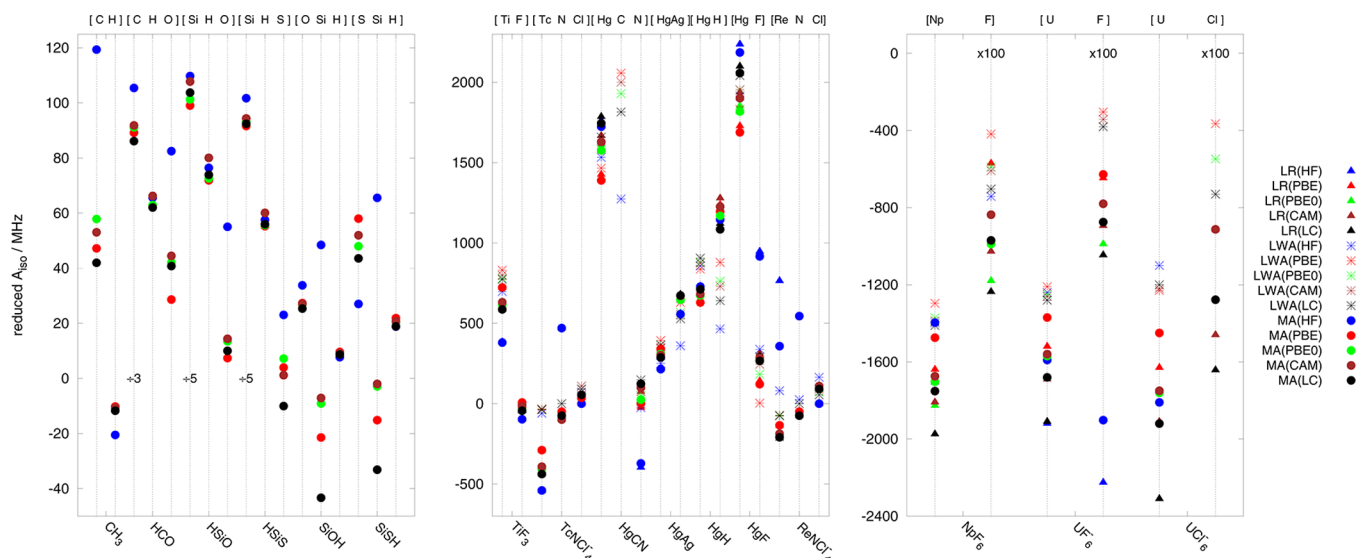


Figure 1. Reduced isotropic hyperfine coupling constants (MHz) for molecule Sets I–III, calculated with different methods (only MA data for molecule Set I). In the plot key, CAM = CAM-B3LYP, LC = LC-PBE0. All calculated HFCs were divided by g_N of the respective nucleus for better comparison. In the center plot (Set II), all Hg data were divided by 10, Re data divided by 5, and data for C, N, F, Cl multiplied by 10. In the other two panels, data were scaled as indicated.

from 2-component second-order DKH calculations, are available for comparison.⁶⁸

From a comparison of the different approaches to extract the HFC from the calculations, it is possible to assess the relative importance of some of the factors that determine the quality of the result. The most important difference between the quasi-restricted version of LWA, as it has been implemented here, and the MA approach is that the latter allows for spin polarization. Likewise, the LR calculations afford spin polarization but treat SO coupling perturbatively only to lowest order. Comparisons of LR and MA are used to assess the importance of SO coupling beyond lowest order, and comparisons of LWA and MA are used to investigate the importance of spin polarization. HFC has a potentially large nonrelativistic limit. One may therefore expect that higher order SO effects are less important for HFC, relatively speaking, as compared to g -shifts which vanish in the absence of SO coupling.

The three methods have different associated computational cost. The scalar relativistic spin-unrestricted step in the LR calculations has the same demands as a nonrelativistic spin-unrestricted SCF calculation once the matrix elements of the relativistic operator are constructed. In our implementation, this step involves a numerical integration and therefore takes roughly the same time as one pure-DFT SCF iteration. The solution of the coupled-perturbed KS equations in the LR framework has roughly the computational cost of three SCF cycles because of the three associated perturbations. Some of the effort can be consolidated and the actual computational effort tends to be somewhat lower. The MA approach as implemented utilizes data from three converged 2-component SCF calculations. The generalized-collinear framework adopted in this setup requires the optimization of four density matrixes instead of two for a scalar spin-unrestricted calculation, and the density matrices have real and imaginary parts. Compared to a scalar spin-unrestricted KS SCF cycle, this gives a formal increase of CPU time by a factor of 4 for each SCF cycle in the MA calculations. Since there is no follow-up coupled-perturbed equation to be solved, the two approaches

can be competitive when using scalar and 2-component implementations that are similarly well optimized. The LWA technique, as implemented here without spin polarization, can be very efficient, since it only requires the optimization of one complex density matrix. The calculations and transformations of magnetic property integrals have comparable costs in each of the approaches.

HFC is known to be sensitive to electron correlation. In DFT calculations, HFC is also known to be sensitive to the treatment of exchange, that is, local exchange functionals vs inclusion of some fraction of exact nonlocal exchange in global and range-separated hybrids. Comparisons between HF and DFT calculations provide information about the importance of electron correlation as well as about deficiencies in the functionals. These two issues are interrelated. For instance, approximate exchange-correlation functionals tend to afford a delocalization error,⁹⁹ which results in covalent chemical bonds and delocalization of orbitals that would formally be classified as lone pairs or nonbonding. This problem is connected with the DFT self-interaction which, in turn, has been shown to mimic the effects from certain classes of electron correlation.^{100,101} Another potential issue is the use of a nonrelativistic approximate spin-density XC functional in relativistic calculations, based on a suitable definition of the spin magnetization.⁵⁶ Finally, there is the use of the density matrix of the noninteracting KS system in place of the density matrix of the interacting system, which is commonplace in magnetic property calculations with DFT. We will not specifically address the latter issue.

For a quick overview of the results, the scatter of the isotropic HFC constants among the different methods is graphically displayed in Figure 1. In many cases, HF theory and the nonhybrid functional PBE, as well as the nonspin-polarized LWA approach, are seen to produce outliers, as discussed in the following sections.

4.2. Set I: Radicals with Light Main Group Atoms. For the systems with light elements, the HFC is dominated by its nonrelativistic limit, with some influence from scalar relativistic effects for the moderately heavy elements Si and S. Spin–orbit

coupling represents a very minor influence. The calculated results for molecule Set I are collected in Table 1. We forego a detailed comparison with experiment. A previous paper from our group reported the LR ZORA hyperfine implementation in NWChem and noted reasonable agreement with experiment in cases where experimental data were available,⁶⁶ when using the PBE0 and CAM-B3LYP hybrid functionals. In some cases, large variations among different classes of functionals were noted for the Set I systems in this previous paper, which is consequently also seen in the present study which additionally includes HF theory and the LR-PBE0 functional. Significant differences are found between the DFT and HF results. Across the range of functionals, the agreement between LR and MA is near perfect. It is noted in passing that *g*-shifts (deviation from the free-electron *g*-value) are entirely due to SO coupling. However, a perturbative treatment to first order, as provided by the LR framework, is sufficient for the Set I molecules to capture such SO effects. Consequently, in Paper I, we also found excellent agreement between LR and MA *g*-factors for Set I.

The quasi-restricted calculations (LWA) are not adequate for a description of electron–nucleus HFC, due to the lack of spin polarization. This is much unlike the often quite satisfactory performance of such calculations for *g*-shifts.^{82,102} This deficiency has, of course, long been known from nonrelativistic calculations, and many different approaches have been proposed in order to circumvent this problem (see the Introduction for a selection of references). In the framework of ZORA calculations of EPR parameters, Stein et al. obtained satisfactory agreement with experiment from DFT calculations on Ni complexes by obtaining the isotropic HFC from spin-polarized scalar relativistic calculations (sampling the FC contribution) and the anisotropic part from quasi-restricted scalar and spin–orbit calculations (sampling the contributions from the SD and the PSO terms).¹⁰³ However, the (dipolar) SD term is also affected by the spin polarization. For example, for CH₃, the isotropic component of the carbon HFC in the PBE0 calculation is 81.3 MHz in the spin-polarized calculations. The LWA calculation gives a perfectly anisotropic tensor, the reason being that the SOMO is a pure carbon 2*p* orbital with no density at C or H that could create an isotropic contribution from the FC term. With the isotropic contribution from LR or MA added to the quasi-restricted PBE0 results, the unique tensor components would be +11.6 and +220.6 MHz. These values agree reasonably well with the spin-polarized PBE0 results when taking the large variations of the HFC components with the functional for this system into consideration, but differences remain. Similarly, for the protons in CH₃ the tensor elements obtained with this procedure would be −99.7, −61.4, and −36.7 MHz (PBE0), which reproduces the signs and roughly the magnitudes of the tensor components from the LR calculation.

As far as the variations between HF and the various functionals are concerned, it is important to keep in mind that HFC is sensitive to the quality of the electronic structure. HF wave functions lack electron correlation and typically suffer from a localization error⁹⁹ (too little covalency in the chemical bonds and not enough delocalization in delocalized systems). KS DFT incorporates electron correlation but with popular functionals this method tends to suffer from delocalization and self-interaction errors (too covalent bonds, too much delocalization).^{99,104} Exchange–correlation functionals are often devised with total energies and binding energies in mind. The quality of these functionals may not be reflected in

the KS orbitals and eigenvalues.^{105–107} As a consequence, different energy functionals that show clear differences for energetics may deliver similar KS orbitals and XC potentials, causing an insensitivity of calculated properties to the functional. Conversely, molecular properties may show large variations among calculations based on different energy functionals that would all be acceptable for relative energies and geometries of stable ground state structures, if those different functionals produce noticeably different KS orbitals and XC potentials. Our results in Table 1 show that for the HFC components of Set I doublets, the variations among the different hybrid functionals are relatively minor. However, there are significant variation between the nonhybrid DFT, hybrid DFT, and HF calculations. This behavior is expected since the KS orbitals and XC potentials are very different between these calculations.

4.3. Set II: Radicals with Transition Metals. Test Set II comprises doublet radicals with light to heavy transition metal atoms (Ti, Tc, Re, Hg). The HFC principal components A_{\perp} , A_{\parallel} for atoms with linear local environments are collected in Table 2 along with isotropic averages. Isotropic HFCs for the F ligand in TiF₃ and the Cl ligands for the Tc and Re complex are provided in Table 5. Experimental data are included for comparison where available. For the molecules in Set II as well as the molecules in Sets I and III, an accurate computational model would require consideration of the environment of the molecule as it was studied experimentally (e.g., in a crystal, in solution, or in a rare gas matrix). Therefore, some deviations from experiment must be expected no matter how accurate the gas phase computations are. However, comparisons with experimental data are useful to identify calculations that are clearly deficient, assuming that perturbations from the molecule's surrounding are not dominating the observed EPR spectra.

As in Set I, in Set II there are noticeable variations of the results with the functional, and when comparing DFT with HF theory. Fluorine is a particularly sensitive and difficult case. Higher order SO effects are showing up in differences between the LR and MA data. In relative terms, however, these differences are significantly smaller than the variations among the different functionals and therefore of secondary importance for test Set II. Some of the stronger effects from SO coupling are calculated for the Hg principal components of the HgH radical. Figure 2 shows results from MA calculations for HgH where the ZORA SO integral matrix used for the ground state SCF is scaled by a factor λ , with $\lambda = 1$ corresponding to the calculations listed in Table 2. Similar scaling techniques have also been used previously in refs 70 and 108 and in Paper I. The nonlinear behavior indicates the influence from higher order SO effects, with SO coupling reducing the magnitude of A_{\perp} and increasing that of A_{\parallel} (leading to a near-perfect cancellation of higher-order SO effects on A_{iso} in the HF calculation). These trends are responsible for the corresponding differences of the LR and MA results for HgH listed in Table 2 (or lack thereof).

At first sight, the case of TiF₃ may seem similar to CH₃ in the sense that the system is planar, with a SOMO orbital perpendicular to the molecule plane (predominantly Ti 3*d*_{z²}, as shown in the graphical abstract). Unlike the CH₃ case, the LWA calculations for TiF₃ produce a large negative isotropic HFC. The nuclear *g*-factor of Ti is negative, and therefore, the negative signs, also found for the LR and MA calculations, are consistent with a positive spin-density at the Ti nucleus. SO

Table 1. Hyperfine Coupling Principal Components (MHz) for Molecule Set I Calculated with the LR, MA, and LWA Approaches and Different Functionals (Point Nuclei)

		HF			PBE			PBE0			CAM-B3LYP			LC-PBE0				
		A ₁₁	A ₂₂	A ₃₃	A ₁₁	A ₂₂	A ₃₃	A ₁₁	A ₂₂	A ₃₃	A ₁₁	A ₂₂	A ₃₃	A ₁₁	A ₂₂	A ₃₃		
CH ₃	C	LR	93.2	93.2	317.3	-13.6	-13.6	226.6	2.5	2.5	239.3	-5.7	-5.7	235.1	-19.5	-19.5	216.3	
	C	MA	92.9	92.9	317.3	-13.8	-13.8	226.6	2.3	2.3	239.4	-5.9	-5.9	235.2	-19.7	-19.7	216.4	
	C	LWA	-52.6	-52.6	105.1	-75.2	-75.2	150.2	-69.7	-69.7	139.3	-69.7	-69.7	139.1	67.2	67.2	134.3	
	H	LR	-157.8	-116.3	-69.7	-96.2	-56.4	-18.3	-105.1	-64.8	-25.9	-99.3	-60.0	-19.6	-105.3	-65.3	-25.9	
	H	MA	-157.8	-116.3	-69.7	-96.2	-56.4	-18.3	-105.1	-64.8	-25.9	-99.3	-60.0	-19.6	-105.3	-65.3	-25.9	
	H	LWA	-21.7	-6.5	28.2	-30.5	-2.9	33.4	-28.6	-3.9	32.4	-28.1	-3.8	31.8	-27.5	-4.2	31.7	
	HCO	C	LR	381.0	406.3	546.3	329.7	336.1	461.6	334.4	343.7	473.9	337.4	345.1	479.2	322.3	322.3	454.9
		C	MA	380.7	406.2	546.4	329.7	335.7	462.0	334.2	343.5	474.2	337.0	345.0	479.4	322.2	322.2	455.0
		C	LWA	241.1	243.9	341.1	315.9	319.2	431.5	294.2	297.4	406.7	294.2	297.5	408.0	275.3	278.6	386.5
H		LR	352.2	358.9	388.5	334.1	342.0	369.7	337.2	344.9	372.7	355.3	362.9	392.2	331.8	339.3	368.4	
H		MA	352.2	359.0	388.5	334.1	342.0	369.7	337.2	344.9	372.7	355.3	362.9	392.1	331.8	339.3	368.4	
H		LWA	284.1	291.3	319.0	293.8	301.3	331.9	291.2	298.6	328.9	292.1	299.4	329.8	282.2	289.5	319.8	
O		LR	-174.3	-19.4	5.9	-129.8	29.3	35.4	-141.9	19.2	26.8	-146.2	19.2	25.4	-141.2	19.8	28.3	
O		MA	-174.4	-19.1	6.0	-130.2	29.4	35.8	-142.1	19.5	27.0	-146.3	19.8	25.5	-141.4	20.3	28.5	
O		LWA	-89.6	-27.8	25.5	-119.1	38.4	40.1	-111.1	34.9	36.8	-113.0	34.4	36.3	-109.5	33.1	35.0	
HSiO	Si	LR	-732.3	-567.8	-528.6	-640.0	-512.7	-497.0	-660.8	-524.7	-501.1	-701.7	-559.1	-533.9	-683.0	-537.3	-507.7	
	Si	MA	-733.1	-567.6	-527.8	-641.1	-512.1	-496.8	-661.9	-524.5	-500.9	-702.6	-558.8	-533.4	-683.9	-537.1	-507.2	
	Si	LWA	-611.0	-498.6	-498.3	-664.0	-545.9	-545.2	-652.7	-534.7	-534.3	-686.9	-565.1	-564.7	-654.3	-533.3	-533.0	
	H	LR	425.0	427.0	428.6	398.3	400.6	406.2	402.7	405.1	409.3	444.4	446.5	451.1	410.4	412.4	416.4	
	H	MA	425.0	427.0	428.6	398.3	400.6	406.2	402.6	404.9	409.2	444.3	446.4	451.1	410.3	412.3	416.2	
	H	LWA	255.7	257.9	267.0	327.5	329.5	339.4	308.0	310.0	319.7	311.8	313.8	323.5	293.9	295.9	305.5	
	O	LR	-124.9	-3.2	2.7	-91.4	36.3	38.2	-97.7	32.8	33.9	-99.3	32.5	33.9	-89.9	32.8	34.3	
	O	MA	-124.9	-2.8	2.7	-91.5	36.2	38.6	-97.8	32.8	34.3	-99.3	32.7	34.0	-90.0	32.9	34.4	
	O	LWA	-54.6	-16.8	16.8	-86.6	36.9	36.1	-77.0	30.3	31.0	-77.6	28.6	29.3	-72.6	25.4	26.0	
HSiS	Si	LR	-687.0	-523.6	-478.7	-596.5	-474.5	-455.4	-614.3	-481.9	-455.7	-626.3	-487.2	-458.6	-622.3	-475.3	-441.5	
	Si	MA	-690.1	-524.2	-480.0	-598.1	-473.0	-455.3	-615.6	-481.3	-455.6	-627.3	-486.6	-458.0	-623.7	-474.8	-441.3	
	Si	LWA	-478.3	-377.4	-374.1	-603.1	-489.6	-485.7	-571.2	-460.0	-456.3	-580.1	-466.1	-462.2	-554.6	-439.6	-435.7	
	H	LR	318.9	322.1	323.7	305.3	307.9	313.2	307.4	310.0	314.5	332.6	335.1	339.6	309.5	312.1	316.4	
	H	MA	318.6	322.0	323.7	305.3	307.9	313.2	307.5	310.2	314.6	332.5	335.1	339.5	309.4	312.0	316.2	
	H	LWA	175.6	178.5	185.5	247.7	250.0	258.1	226.8	229.3	237.1	223.2	225.7	233.5	210.7	213.4	221.2	
	S	LR	-27.8	-26.7	85.0	-35.7	-35.1	76.2	-34.9	-34.0	78.6	-41.6	-38.3	81.3	-42.4	-41.1	70.5	
	S	MA	-28.1	-27.2	85.0	-35.6	-35.5	76.2	-35.0	-34.5	78.9	-41.7	-38.6	81.8	-42.5	-41.4	70.9	
	S	LWA	-23.6	-23.5	59.8	-32.6	-31.1	78.4	-29.9	-28.7	72.8	-30.4	-29.3	75.9	-27.9	-26.9	71.1	
SiOH	O	LR	-40.7	-19.6	-15.9	-38.4	-13.4	-10.5	-37.4	-12.8	-10.5	-37.7	-11.3	-11.2	-36.4	-10.5	-9.3	
	O	MA	-40.8	-20.2	-15.9	-38.7	-13.3	-10.0	-37.4	-13.2	-10.4	-37.7	-12.6	-11.2	-36.5	-12.0	-9.2	
	O	LWA	-18.4	-8.5	-4.4	-44.1	-11.2	-4.2	-38.9	-9.0	-3.4	-35.7	-22.0	-13.8	-27.9	-19.1	-10.6	
	Si	LR	-260.3	35.8	67.6	-181.5	114.5	136.5	-196.6	101.3	127.5	-208.9	104.9	137.6	-166.6	138.2	173.7	

Table 1. continued

	HF			PBE			PBE0			CAM-B3LYP			LC-PBE0			
	A ₁₁	A ₂₂	A ₃₃	A ₁₁	A ₂₂	A ₃₃	A ₁₁	A ₂₂	A ₃₃	A ₁₁	A ₂₂	A ₃₃	A ₁₁	A ₂₂	A ₃₃	
SiOH																
Si	MA	-261.8	36.7	63.8	-186.2	118.6	138.9	-198.7	103.4	125.7	-210.7	106.5	127.8	-163.2	139.4	168.2
Si	LWA	-132.2	38.2	61.0	-221.1	125.6	189.5	-253.2	142.3	226.1	-149.3	18.2	59.7	-148.7	4.0	62.5
H	LR	36.4	39.9	53.1	47.3	50.8	63.4	44.0	47.5	60.4	44.3	48.0	61.6	41.5	45.1	58.2
H	MA	36.4	39.8	53.2	47.3	50.8	63.3	44.0	47.4	60.4	44.3	47.9	61.8	41.5	45.1	58.5
H	LWA	28.7	32.0	45.2	44.0	47.5	59.0	38.8	42.0	50.0	34.8	37.8	58.5	35.7	39.2	56.0
SiSH																
S	LR	7.4	8.1	18.8	20.6	24.1	30.0	16.8	18.9	26.1	19.3	20.1	27.4	15.5	16.1	24.5
S	MA	7.7	8.3	18.9	20.5	24.1	30.1	16.9	18.9	26.1	19.4	20.2	27.4	15.5	16.1	24.5
S	LWA	14.6	15.4	20.8	33.0	33.3	38.3	27.2	27.4	32.5	25.4	25.6	31.3	22.4	23.1	29.6
Si	LR	-280.2	18.1	44.7	-181.0	106.1	124.2	-198.4	93.7	113.7	-211.8	100.2	120.9	-173.4	129.7	153.3
Si	MA	-281.7	19.1	44.3	-184.7	109.3	125.7	-200.2	95.8	114.1	-213.5	101.9	118.1	-174.9	130.9	154.4
Si	LWA	-157.2	86.8	119.6	-194.3	101.6	115.6	-182.3	95.5	110.3	-187.8	98.1	112.0	-179.0	93.7	108.4
H	LR	102.1	102.6	110.7	119.4	120.2	127.2	111.3	112.0	119.0	112.9	114.0	120.2	102.8	103.8	110.3
H	MA	102.2	102.7	110.6	119.5	120.2	127.2	111.4	112.1	119.0	113.0	114.1	120.4	102.8	103.8	110.3
H	LWA	62.9	65.1	69.6	103.7	106.4	111.1	90.7	93.4	98.1	85.2	87.7	92.5	80.4	83.1	87.5

coupling is not strong in this system, and consequently the PSO mechanism contributes very little to the isotropic Ti HFC (+3 MHz). The anisotropy of the HFC at Ti is relatively small. The reason for the nonvanishing isotropic FC mechanism in the LWA calculations is a roughly 12% Ti 4s character of the SOMO (LR/PBE0),⁶⁶ which gives a contact spin-density at Ti when one of the frontier orbitals that is fractionally occupied during the SCF is selected as the SOMO for the purpose of evaluating the HFC. The lack of spin-polarization in the LWA calculations, however, leads to a strong overestimation of the HFC relative to the spin-polarized LR and MA calculations, in particular at the HF level (by 83% for A_{iso}). For pure DFT, the percentage deviations between spin-restricted and spin-polarized results are less pronounced (PBE, 15% for A_{iso}). Pure DFT overestimates the Ti HFC magnitude, while the hybrid-DFT LR and MA calculations perform satisfactorily when compared to experiment. Figure S1 in the SI provides numerical data for the extent of the DFT delocalization error for TiF₃ (and the large localization error for HF) related to the SOMO. The LC-PBE0 calculations result in small curvatures in plots of the energy versus fractional electron numbers around the electron number for the neutral radical, which indicates that the delocalization error for TiF₃ is small with this functional. Thus, the good agreement of the HFC data calculated with this functional and experiment may not be accidental. With the PBE0 functional, delocalization is pronounced, yet the LR and MA calculations give acceptable HFCs (though likely less accurate than LC-PBE0). This shows that the extent of delocalization is not the only factor that determines the quality of the result. Assuming that the isotropic fluorine HFC (Table 5) is negative, the LC-PBE0 calculation gives the best agreement with experiment while HF theory and the other functionals perform poorly. The variations among the experimental data for TiF₃, obtained in different 'inert' noble gas matrices, demonstrate nonvanishing effects from the molecular environment.

The 4d metal radical TcNCl₄⁻ exhibits qualitatively similar behavior as TiF₃ regarding the functional trends. The quasi-restricted LWA calculations produce mainly the dipolar contribution. These systematically underestimate the magnitude of the HFC components and are not discussed further. Spin polarization is evidently very important in this system, rendering the Tc HFC negative (g_N is positive). The lack of correlation, and the localization error, in HF leads to a significant overestimation of the HFC principal components with respect to experiment (LR and MA), while the delocalization error in PBE leads to a strong underestimation. Upon inclusion of nonlocal exact exchange in the KS operator, either in a range-separated manner (CAM-B3LYP and LC-PBE0) or globally (PBE0), the results improve. LC-PBE0 performs best in comparison with experiment.

For the doublets with a 5d metal (HgH, HgF, HgAg, ReNCl₄⁻), variational inclusion of SO coupling in the reference Hamiltonian (MA vs LR) leads with few exceptions to changes of the HFC magnitudes both for the metal and ligand atoms on the order of a few percent. The effects on the tensor components for HgH exceed 5% in several cases. The HF calculations for ReNCl₄⁻ show large differences between LR and MA. However, as we already noted in Paper I, the LR/HF calculation for this system affords serious spin contamination (S² = 0.943 instead of the expected 0.750), and therefore, the HF calculations are unreliable. The DFT calculations exhibit only slight deviations from 0.750 in the scalar relativistic

Table 2. Hyperfine Coupling Matrix Components (MHz) for Molecule Set II Calculated with the LR, MA, and LWA Approach and Different Functionals (Gaussian Nuclear Model)^a

	HF			PBE			PBE0			CAM-B3LYP			LC-PBE0		
	A_{\perp}	A_{\parallel}	A_{iso}	A_{\perp}	A_{\parallel}	A_{iso}	A_{\perp}	A_{\parallel}	A_{iso}	A_{\perp}	A_{\parallel}	A_{iso}	A_{\perp}	A_{\parallel}	A_{iso}
TiF ₃															
Ti															
LR	-112	-137	-121	-219	-247	-228	-185	-214	-195	-188	-222	-199	-174	-206	-185
MA	-112	-137	-120	-219	-248	-228	-185	-214	-194	-188	-221	-199	-174	-206	-185
LWA ^f	-207	-247	-220	-247	-292	-262	-231	-277	-246	-237	-283	-252	-228	-276	-244
<i>b</i> _{expt.} ¹¹¹	-178	-198	-185												
<i>c</i> _{expt.} ¹¹¹	-169	-193	-177												
TcNCl ₄ ⁻															
Tc															
LR	-458	-1136	-684	-227	-644	-366	-361	-817	-513	-336	-816	-496	-391	-875	-553
MA	-460	-1128	-682	-223	-650	-365	-359	-818	-512	-334	-816	-495	-391	-877	-553
LWA ^f	103	-430	-75	109	-340	-41	108	-349	-44	112	-362	-46	111	-367	-48
<i>c</i> _{expt.} ¹¹²	-408	-878	-565												
N															
LR	33	-9	19	-3	1	-2	-6	2	-4	-6	2	-4	-7	4	-3
MA	33	-9	19	-3	1	-2	-6	2	-3	-6	2	-4	-7	4	-3
LWA	1	0	0	-1	1	0	-1	1	0	-1	1	0	-1	1	0
ReNCl ₄ ⁻															
Re															
LR	5206 ^e	4354	4922	-548	-1563	-886	-905	-1995	-1268	-860	-2008	-1243	-1004	-2158	-1389
MA	2078	2758	2305	-506	-1581	-864	-869	-1954	-1231	-827	-1961	-1205	-967	-2097	-1344
LWA ^f	126	1313	521	-135	-1109	-460	-136	-1135	-469	-140	-1173	-484	-140	-1174	-485
<i>c</i> _{expt.} ¹¹³	-1172	-2308	-1551												
N															
LR	49	212	103	-3	1	-2	-6	2	-3	-6	2	-3	-6	3	-3
MA	29	9	22	-3	0	-2	-6	1	-3	-6	1	-3	-6	3	-3
LWA	0	1	1	0	0	0	0	1	0	0	1	0	0	1	0
HgH															
Hg															
LR	7155	7841	7384	6212	7114	6513	6645	7514	6935	6749	7654	7051	7008	7929	7315
MA	6954	8204	7371	5715	7674	6368	6236	7966	6813	6345	8043	6911	6641	8329	7203
LWA	8070	9888	8676	7681	10047	8469	8129	10423	8894	8080	10414	8858	8370	10758	9166
<i>c</i> _{expt.} ¹¹⁴	6608	7790	7002												
H															
LR	664	650	659	694	688	692	677	669	674	717	709	714	630	619	626
MA	643	632	640	670	663	668	656	648	653	693	670	685	604	610	606
LWA	259	263	260	491	492	491	425	426	426	408	409	408	357	359	358
<i>c</i> _{expt.} ¹¹⁴	711	707	710												
HgF															
Hg															
LR	22597	22679	22624	17371	17701	17481	18661	18917	18746	19519	19783	19607	21149	21405	21235
MA	22040	22255	22111	16870	17514	17085	18228	18720	18392	19072	19568	19238	20657	21140	20818
LWA	19136	19845	19373	18250	19069	18523	19480	20333	19764	19481	20352	19771	20358	21251	20656
<i>b</i> _{expt.} ¹¹⁰	21880	22622	22127												
F															
LR	117	1261	498	-580	1380	74	-448	1387	164	-415	1321	164	-354	1172	155
MA	98	1252	482	-657	1482	64	-482	1405	147	-440	1326	149	-375	1168	140
LWA ^f	7	521	178	-680	1366	2	-389	1067	96	-321	1029	129	-233	924	153
<i>c</i> _{expt.} ¹¹⁰	195	1344	578 ^h												

Table 2. continued

	HF			PBE			PBE0			CAM-B3LYP			LC-PBEO		
	A_{\perp}	A_{\parallel}	A_{iso}	A_{\perp}	A_{\parallel}	A_{iso}	A_{\perp}	A_{\parallel}	A_{iso}	A_{\perp}	A_{\parallel}	A_{iso}	A_{\perp}	A_{\parallel}	A_{iso}
HgCN															
Hg															
LR	17704	18095	17834	14200	14895	14432	16102	16740	16315	16652	17309	16871	17849	18511	18070
MA	17186	17948	17440	13574	15030	14060	15517	16795	15943	16068	17328	16488	17233	18483	17650
LWA	15071	16379	15507	14283	15911	14826	15476	17079	16010	15545	17185	16091	16229	17899	16786
$\epsilon_{\text{expt.}}^{115}$	15390	16770	15850												
C															
LR	495	478	489	339	404	361	376	427	393	405	455	422	371	411	384
MA	483	470	479	325	390	347	362	416	380	391	443	408	357	401	372
LWA	170	197	179	266	334	289	253	307	271	263	315	281	241	285	255
N															
LR	-28	9	-16	-6	11	-1	-4	12	1	-1	13	3	1	14	5
MA	-28	9	-15	-5	9	0	-3	11	1	-1	12	4	1	13	5
LWA ^f	-5	7	-1	0	9	3	-2	8	2	-4	9	0	5	9	6
HgAg															
Hg															
LR	2129	2330	2196	3428	3720	3525	3101	3383	3195	3034	3301	3123	2879	3147	2968
MA	2038	2446	2174	3221	3914	3452	2922	3539	3128	2873	3419	3055	2729	3268	2909
LWA	2309	2993	2537	3714	4509	3979	3411	4232	3684	3265	4067	3533	3403	4287	3698
$\epsilon_{\text{expt.}}^{116}$	2520	3130	2723												
Ag															
LR	-1277	-1270	-1275	-1490	-1491	-1490	-1483	-1483	-1483	-1540	-1538	-1539	-1545	-1541	-1544
MA	-1267	-1262	-1265	-1470	-1473	-1471	-1467	-1469	-1467	-1525	-1526	-1525	-1529	-1529	-1529
LWA	-819	-820	-819	-1429	-1433	-1431	-1288	-1291	-1289	-1261	-1264	-1262	-1198	-1200	-1199
$f_{\text{c-expt.}}^{116}$	-1562	-1562	-1562												

^aSee Table 5 for additional data. ^bNeon matrix. ^cArgon-matrix. Signs of principal components were not determined. Definition of A_{iso} in Reference 110 excludes PSO mechanism. ^dThe experiment assumes the signs of principal components to be same as the nuclear magnetic moments. ^eSingle crystal ESR spectra. Experiment did not provide signs. ^fSome or all signs have been set to match the LR results. ^gHartree-Fock data for ReNCl_4^- are unreliable because of spin-contamination. ^hAssuming positive A_{\perp} , A_{\parallel} .

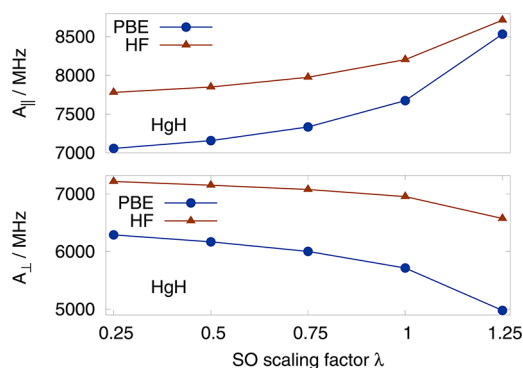


Figure 2. Hyperfine tensor components for ^{199}Hg in HgH from calculations where the SO operator is scaled by a factor λ . MA approach.

calculations; see Table S5 in the SI (data for all other systems are also provided). As pointed out by Perdew et al., some spin contamination of the KS determinant is needed to describe the spin density of the correlated system.¹⁰⁹ For ReNCl_4^- , the spin-polarized pure DFT calculation (PBE) severely underestimates the isotropic HFC and the principal components. Including exact exchange remedies the problem to a large degree, although even the LC-PBE0 result does not agree with experiment as well as it does for the Tc system.

The Hg hyperfine couplings are discussed in the following subsection in the context of finite-nucleus effects. The LWA calculations perform reasonably well for the HFC of Hg itself, unlike most other cases where deviations between LWA and spin-polarized calculations by factors of 2, 3, or more are found. This is likely a consequence of the dominant *s*-character of the SOMO at Hg, which renders a spin-polarization mechanism less influential on a relative scale.

Some ligand data for the Hg systems are noteworthy. For the silver HFC in HgAg, the spin-polarized DFT calculations with range-separated hybrid exchange functionals give excellent agreement with experiment. The negative signs are consistent with a positive spin density at the nucleus since g_N is negative. For the proton HFC in HgH, CAM-B3LYP performs a bit better than LC-PBE0 in reproducing the experimental value, and PBE0 PBE and HF are also close. As pointed out above, the molecular environment may influence the experimental data. None of the theory level produces a clear outlier for the ^1H HFC of HgH (LR, MA). It is not clear which functional is the most accurate in this case.

The experimental HFC of the ^{19}F nucleus in HgF is clearly very difficult to reproduce by the calculations. Among PBE, the three hybrid functionals, and HF theory, the calculated isotropic HFCs span an order of magnitude. The HF results (LR and MA) are closest to experiment and also reproduce the large anisotropy of the HFC. In the PBE results there is practically no isotropic contribution; the large principal components for ^{19}F are seen to cancel almost perfectly. If the sign of A_{\perp} is correctly predicted by the hybrid DFT calculations, the isotropic HFCs, although much improved from the nonhybrid DFT calculations, are too small by a factor of 4. It is tempting to reassign A_{\perp} in these calculations as positive as this would lead acceptable agreement with experiment for A_{iso} . It is conceivable that the experimental value is more sensitive to influences from the environment than the corresponding fluorine HFC of TiF_3 . Figure S2 in the SI shows a fractional electron plot for HgF indicating substantial

delocalization errors with PBE, PBE0, and CAM-B3LYP, and an essentially perfect behavior for LC-PBE0. HF theory gives a pronounced localization error for the SOMO, although smaller than for TiF_3 . It may be the case that the experimental assignment of A_{iso} should be revised. Knight et al.¹¹⁰ pointed out that the signs of A_{\perp} and A_{\parallel} were assumed to be positive. If the sign of the experimental A_{\perp} were negative as in the hybrid DFT calculations, the average of the HFC principal components would be 318 MHz, assuming that none of the other parameters that are part of the analysis of the experimental spectrum is affected.

4.4. Effects from Finite Nuclear Volumes. The hyperfine operator probes the electronic structure very close to the nucleus. It is known that finite nuclear volume effects on HFC and other properties involving relativistic analogs of non-relativistic contact-type operators can be very significant (e.g., hyperfine coupling, *J*-coupling, Mössbauer isomer shifts).^{19,68,77,81,117} Moreover, point nuclei may introduce unwanted (near-) singularities in property operators that can be difficult to handle numerically. Finite-nucleus corrections are expected to be particularly large when the property of interest is determined by orbitals with large *s* character centered on the heavy element. Therefore, the radicals containing Hg are ideal test cases for calculating finite-nucleus corrections on hyperfine coupling.

Calculated HFC constants and principal components for the four Hg systems of molecule Set II obtained from MA calculations are collected in Table 3. Across the board, there is a significant reduction of the HFC components and of the isotropic average when a finite-nucleus model is adopted. For best comparison with the benchmark data from ref 68, calculations with the BP functional were also performed (last column in Table 3), in addition to the other functionals used in this work. We discuss the BP data first. For HgH, HgF, HgCN, and HgAg, our FN results agree reasonably well with the four-component calculations from ref 68, which obtained isotropic FN hyperfine couplings of 5906, 16810, 13875, and 3288 MHz, respectively. The relative finite-nucleus corrections in our BP calculations amount to a reduction of the HFC by 15, 15, 15, and 12%, respectively, for these systems. The order of magnitude is comparable to the range of 11–15% reported in ref 68 for the four-component calculations (15, 11, 11, 11) and also consistent with finite-nucleus effects that we previously reported for LR hyperfine calculations within the ZORA framework.⁷⁷ This range is below the magnitude of FN effects obtained with the DKH2 operator as reported in ref 68 (12–17%). DKH2 also consistently gave too large HFC constants. In terms of best agreement with experiment, the very significant reductions of the HFC due to switching from DKH2 to four-component or ZORA calculations, and to finite nuclei, expose other approximations in the calculations: the FN BP calculations severely underestimate experiment for HgF and HgCN. For HgH, the FN BP calculations also underestimate the experimental A_{iso} , whereas for HgAg the FN effect produces a welcome reduction toward experiment. The data in Table 3 show that adopting one of the functionals with global (PBE0) and range-separated exchange (CAM-B3LYP, LC-PBE0) tends to improve the results toward experiment, by further lowering the isotropic HFC for HgAg and increasing those of the other three systems.

4.5. Set III: Small Actinide-Containing Radicals. Computed results for the systems containing actinides (An) are collected in Table 4. For the metal centers, the HFC is

Table 3. Comparison ^{199}Hg Hyperfine Coupling Constants (MHz) for Hg Containing Radicals^a

	HF			PBE			PBE0			CAM-B3LYP			LC-PBE0			BP		
	A_{\perp}	A_{\parallel}	A_{iso}	A_{\perp}	A_{\parallel}	A_{iso}	A_{\perp}	A_{\parallel}	A_{iso}	A_{\perp}	A_{\parallel}	A_{iso}	A_{\perp}	A_{\parallel}	A_{iso}	A_{\perp}	A_{\parallel}	A_{iso}
HgH																		
PN	8100	9368	8523	6679	8680	7346	7164	8923	7750	7285	9011	7861	7621	9333	8191	6795	8835	7475
FN	6986	8241	7404	5710	7680	6366	6238	7975	6817	6347	8051	6915	6646	8339	7210	5819	7829	6488
expt. ¹¹⁴	6608	7790	7002															
HgF																		
PN	25425	25335	25395	19282	19926	19497	20850	21339	21013	21794	22287	21958	23630	24110	23790	19182	19839	19403
FN	22148	22354	22217	16779	17418	16992	18176	18661	18338	19008	19496	19171	20617	21092	20775	16708	17358	16926
expt. ¹¹⁰	21880	22622	22127															
HgCN																		
PN	19831	20591	20085	15635	17107	16125	17866	19157	18296	18492	19765	18916	19841	21102	20261	15532	17015	16026
FN	17242	18000	17495	13537	14994	14023	15493	16769	15919	16041	17298	16460	17221	18467	17636	13458	14925	13947
expt. ¹¹⁵	15390	16770	15850															
HgAg																		
PN	2244	2670	2386	3589	4293	3823	3254	3881	3463	3218	3774	3404	3023	3570	3205	3527	4229	3761
FN	2079	2494	2217	3169	3862	3400	2935	3553	3141	2910	3462	3094	2797	3338	2977	3124	3810	3353
expt. ¹¹⁶	2520	3130	2723															

^aComparison of Gaussian finite nucleus model (FN) vs. point nucleus (PN) calculations. MA approach. Basis sets as described in the Computational Details section.

Table 4. Actinide Hyperfine Coupling Constants (MHz) for Molecule Set III Calculated with the LR, MA, and LWA Approach and Different Functionals (Gaussian Nuclear Model)

	HF	PBE	PBE0	CAM ^a	LC-PBE0
NpF ₆					
LR	−2142	−2059	−2294	−2272	−2480
MA	−1754	−1852	−2139	−2103	−2200
LWA	−1755	−1628	−1722	−1742	−1772
expt. ¹¹⁸	−1994				
UF ₆ [−]					
LR	192	152	168	169	191
MA	159	137	157	156	168
LWA	124	121	125	126	128
UCl ₆ [−]					
LR	248	163	191	191	231
MA	181	145	176	175	192
LWA	110	123	122	122	120

^aCAM-B3LYP functional.

isotropic and therefore only one value per calculation is given. Additional data for ligand atoms are provided in Table 5. We note that the metal HFC constants in the actinide test set are dominated by contributions from the PSO term. The change in sign and magnitude from Np to U is due to the different signs and magnitudes of the g_N . Figure 1 shows that for the reduced

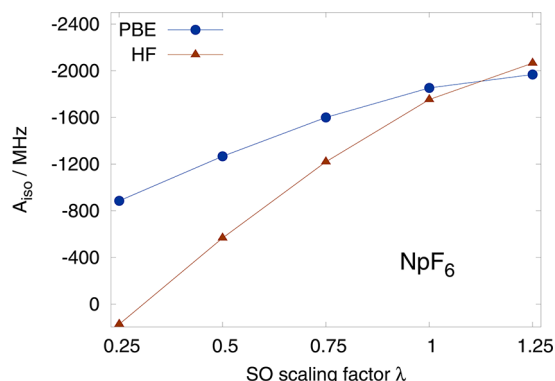
Table 5. Isotropic Hyperfine Coupling (MHz) for selected Ligand Atoms of Radicals from Sets II and III Calculated with the LR, MA, and LWA Approach and Different Functionals (Gaussian Nuclear Model).

	HF	PBE	PBE0	CAM	LC-PBE0
TiF ₃					
F LR	−51	4	−14	−9	−23
MA	−51	4	−14	−9	−23
LWA	−12	−11	−15	−16	−17
^{a,c} expt. ¹¹¹	24				
^{b,c} expt. ¹¹¹	22				
TcNCl ₄ [−]					
Cl LR	0	2	3	3	2
MA	0	2	3	3	3
LWA	4	3	6	6	5
ReNCl ₄ [−]					
Cl LR	0	6	6	6	5
MA	0	5	6	6	5
LWA	9	5	4	3	3
NpF ₆					
F LR	−250	−30	−62	−54	−65
MA	−208	−44	−52	−44	−51
LWA	−39	−22	−31	−32	−37
expt. ¹¹⁸	−72.7				
UF ₆ [−]					
F LR	−117	−34	−52	−47	−55
MA	−100	−33	−46	−41	−46
LWA	−16	−16	−18	−18	−20
UCl ₆ [−]					
Cl LR	−17	−5	−9	−8	−9
MA	−14	−5	−7	−5	−7
LWA	−4	−2	−3	−4	−4

^aNeon matrix. ^bArgon-matrix. ^cSign not determined.

HFCs the sign, magnitude, and functional trends are comparable. HFC principal components computed with the LR approach differ significantly from those calculated with MA, in particular with HF theory, but also with the density functional methods. The difference indicates the importance of higher-order SO effects for these systems. The SOMO, in each case, is at the scalar relativistic level a relatively pure An $5f_{xyz}$ orbital (shown in the graphical abstract for NpF₆).

Previously, Case¹¹⁹ performed Dirac scattered-wave calculations for NpF₆ and obtained HFC constants of −2020 MHz for Np and −63 MHz for F. SO coupling is strong in the An $5f$ shell, and it qualitatively alters the nature of the metal–ligand interactions.¹¹⁹ Despite the strong SO coupling, in our previous work reporting the LR implementation, we showed for NpF₆ that the perturbational approach is able to reproduce the order of magnitude of the metal HFC. For instance, for NpF₆ in the LR calculations, about −2100 MHz of the roughly −2300 MHz (PBE0) coupling constant stem from the PSO-SO linear response term and the remainder from the relativistic analog of the FC+SD mechanism.⁶⁶ The comparison with the MA data indicates that the LR approach systematically overestimates the magnitude of the SO term. Figure 3 shows results from MA

**Figure 3.** Hyperfine coupling constant for ²³⁷Np in NpF₆ calculated with the SO operator scaled by a factor λ . MA approach.

calculations for NpF₆ system where the ZORA SO integral matrix used for the ground state SCF is scaled by a factor λ , with $\lambda = 1$ corresponding to the calculations listed in Table 4. The LR results would give a strictly linear behavior. The higher order SO effects are evident from the nonlinearity of the plots, which is seen to reduce the magnitude of A_{iso} compared to LR, consistent with the LR vs MA comparisons in Table 4.

For the metal hyperfine couplings, the LWA approach is rather insensitive to the choice of XC potential compared to LR and MA. The reasons both for the importance of higher order SO effects and for the at least qualitatively correct performance of the quasi-restricted calculations are likely the same. As we pointed out, the metal HFC constants are dominated by genuine SO contributions via the PSO mechanism which, similar to g-factors (Paper I), are somewhat less sensitive to spin-polarization than mechanisms that depend on contact spin-densities or relativistic versions thereof.

The ligand HFC constants for Set III (Table 5) exhibit comparable tendencies for the three systems: Large magnitudes with HF theory in the spin-polarized calculations (LR, MA), small magnitudes with pure DFT, and an increase from PBE to the hybrid functionals. Spin-polarization is important for correct predictions of the ligand HFC. The quasi-restricted

LWA approach systematically underestimates the magnitude of the halide couplings. The signs of the higher order SO effects are depending on the XC potential. With PBE the magnitude of the ligand coupling constants increases (NpF_6) or remains roughly the same (U systems) when going from LR to MA, while for HF and the hybrid functionals there is a systematic decrease in the magnitude. Experimental data are available for NpF_6 . Among the functionals, for the MA approach PBE0 and LC-PBE0 agree best with experiment. The LC calculation with LC-PBE0 comes even closer, but the same calculation is seen to overestimate the Np coupling constant quite strongly (Table 4). It is worthwhile to reiterate that, since the measurements were not obtained from gas phase, some disagreement with experiment must be expected. Overall, the MA approach with a hybrid functional (preferably with range-separated exchange) appears to be suitable for at least semiquantitative predictions and analyses of the Set III systems, similar to what is found for the molecules in Sets I and II.

5. SUMMARY AND CONCLUSIONS

Two-component relativistic calculations with and without SO coupling variationally included in the ground state Hamiltonian were used to assess different approaches for calculations of hyperfine coupling in DFT calculations. In cases where the SOMO has appreciable *s*-character (e.g., radicals with paramagnetic transition metal centers), calculations utilizing the quasi-restricted setup without spin-polarization may give qualitatively correct answers. Likewise, qualitatively correct answers may be obtained from such calculations on systems with very heavy elements in cases where the PSO mechanism dominates the results.

Both HFC calculations with the LR and the MA approach appear to be suitable for systems with transition metals, even heavy ones. For coupling constants of heavy atoms, finite nucleus corrections should be included. Significant errors from treating SO coupling as a linear perturbation may be expected for cases where SO coupling is strong, either because of high nuclear charges or when there are near-degeneracies (or both). For systems with near-degeneracies the results based on a single reference method such as KS DFT (with approximate functionals) may be unreliable because of a strong multi-reference character of the system.

For the actinide systems in the test set, higher-order SO effects both for metal and ligand HFC are very important because of the very high nuclear charges and the concomitant large relativistic effects. For the metals, the PSO spin-orbit terms dominate the coupling constants. The LR approach in this case overestimates the magnitude of this mechanism. For the ligand nuclei in these systems, the SO effects and trends from different functionals show an interdependence that is reminiscent of a strong cross-dependence previously found for the calculated *g*-factors (Paper I).⁶⁹

A strong sensitivity of the calculated HFC data on the electronic structure model is found in particular in the spin-polarized calculations in cases where there are sizable isotropic contributions from the FC mechanism. ¹⁹F couplings are particularly sensitive. The computations with hybrid functionals with range-separated exchange (LR-PBE0 or CAM-B3LYP) generally appear to perform acceptably well in most scenarios. In some cases, the extent of the DFT delocalization error can be linked to the quality of the calculated results. This error tends to be significantly smaller for hybrid functionals with range-separated exchange that afford an asymptotically correct

XC potential (long-range corrected functionals), as compared to global hybrids and nonhybrid functionals.

Combining the present results with those from Paper I, we conclude that MA-type calculations of EPR parameters with a hybrid functional with range-separated exchange offers a suitable trade-off between accuracy and computational efficiency for systems where high-accuracy correlated wave function methods are computationally too demanding. For hyperfine coupling, where higher order SO effects tend to be less important than for *g*-factors on a relative scale, the LR approach offers a suitable alternative in many cases but should be avoided for very heavy elements such as actinides.

■ ASSOCIATED CONTENT

Supporting Information

Computational results for molecule Set I with point nuclei and finite nuclei. Computational results for molecule Sets II and III with point nuclei. Comparison of results for Set III with different geometries. Figures showing the extent of the DFT delocalization error for TiF_3 and HgF . S^2 values from scalar ZORA calculations. This material is available free of charge via the Internet at <http://pubs.acs.org>.

■ AUTHOR INFORMATION

Corresponding Author

*E-mail: jochena@buffalo.edu.

Notes

The authors declare no competing financial interest.

■ ACKNOWLEDGMENTS

This research was supported by the U.S. Department of Energy, Office of Basic Energy Sciences, Heavy Element Chemistry program, under Grant No. DE-FG02-09ER16066. We further acknowledge support by the Center for Computational Research (CCR) at the University at Buffalo. J.A. thanks Professor Christoph van Wüllen for stimulating discussions at the 2012 Mariapfarr workshop and at the 2012 Chemistry and Physics of the Heavy Elements symposium in Santa Fe. Further, J.A. thanks Dr. Erik van Lenthe for correspondence on the topic of EPR calculations.

■ REFERENCES

- (1) Atherton, N. M. *Principles of Electron Spin Resonance*; Ellis Horwood series in physical chemistry; Prentice Hall: New York, 1993; pp 38, 59–129.
- (2) Moon, S.; Patchkovskii, S. First-principles calculations of paramagnetic NMR shifts. In *Calculation of NMR and EPR Parameters. Theory and Applications*; Kaupp, M.; Bühl, M.; Malkin, V. G., Eds.; Wiley-VCH: Weinheim, 2004; pp 325–338.
- (3) Rinkevicius, Z.; Vaara, J.; Telyatnyk, L.; Vahtras, O. *J. Chem. Phys.* **2003**, *118*, 2550–2561.
- (4) Abragam, A.; Bleaney, B. *Electron Paramagnetic Resonance of Transition Ions*; Clarendon Press: Oxford, 1970; pp 133–216, 650–653.
- (5) Fermi, E. Z. *Phys.* **1930**, *60*, 320–333.
- (6) Breit, G. *Phys. Rev.* **1931**, *37*, 51–52.
- (7) Rosenthal, J. E.; Breit, G. *Phys. Rev.* **1932**, *41*, 459–470.
- (8) Crawford, M. F.; Schawlow, A. L. *Phys. Rev.* **1949**, *76*, 1310–1317.
- (9) Bohr, A.; Weisskopf, V. F. *Phys. Rev.* **1950**, *77*, 94–98.
- (10) Bohr, A. *Phys. Rev.* **1951**, *81*, 331–335.
- (11) Stroke, H. H.; Blin-Stoyle, R. J.; Jaccarino, V. *Phys. Rev.* **1961**, *123*, 1326–1348.

- (12) Rosenberg, H. J.; Stroke, H. H. *Phys. Rev. A* **1972**, *5*, 1992–2000.
- (13) Pyykkö, P. *Lecture Notes in Chemistry: Relativistic Theory of Atoms and Molecules*; Springer: Berlin, 1993; Vol. 60.
- (14) Eriksson, L. A. ESR Hyperfine Calculations. In *Encyclopedia of Computational Chemistry*; von Ragué Schleyer, P., Ed.; Wiley: Chichester, U.K., 1998; pp 952–958.
- (15) Liu, W. *Mol. Phys.* **2010**, *108*, 1679–1706.
- (16) Saue, T. *ChemPhysChem* **2011**, *12*, 3077–3094.
- (17) Pyykkö, P. *Annu. Rev. Phys. Chem.* **2012**, *63*, 45–64.
- (18) Autschbach, J. J. *Chem. Phys.* **2012**, *136*, 150902–15.
- (19) Malkin, E.; Malkin, I.; Malkina, O. L.; Malkin, V. G.; Kaupp, M. *Phys. Chem. Chem. Phys.* **2006**, *8*, 4079–4085.
- (20) Pyykkö, P., private communication.
- (21) Dyall, K. G.; Fægri, Jr., K. *Relativistic Quantum Chemistry*; Oxford University Press: New York, 2007; pages 233–260.
- (22) Reiher, M.; Wolf, A. *Relativistic Quantum Chemistry. The Fundamental Theory of Molecular Science*; Wiley-VCH: Weinheim, 2009.
- (23) Munzarová, M.; Kaupp, M. J. *Phys. Chem. A* **1999**, *103*, 9966–9983.
- (24) Kaupp, M.; Köhler, F. H. *Coord. Chem. Rev.* **2009**, *253*, 2376–2386.
- (25) McConnell, H. M. J. *Chem. Phys.* **1956**, *24*, 764–766.
- (26) Bersohn, R. J. *Chem. Phys.* **1956**, *24*, 1066–1070.
- (27) McLachlan, A. D.; Dearman, H. H.; Lefebvre, R. J. *Chem. Phys.* **1960**, *33*, 65–70.
- (28) Karplus, M.; Fraenkel, G. K. J. *Chem. Phys.* **1961**, *35*, 1312–1323.
- (29) Pople, J. A.; Beveridge, D. L.; Dobosh, P. A. J. *Am. Chem. Soc.* **1968**, *90*, 4201–4209.
- (30) Chipman, D. M. J. *Chem. Phys.* **1979**, *71*, 761–768.
- (31) Chipman, D. M. *Theor. Chem. Acc.* **1992**, *82*, 93–115.
- (32) Sekino, H.; Bartlett, R. J. J. *Chem. Phys.* **1985**, *82*, 4225–4229.
- (33) Kristiansen, P.; Veseth, L. J. *Chem. Phys.* **1986**, *84*, 2711–2719.
- (34) Kossman, S.; Neese, F. J. *Phys. Chem. A* **2010**, *114*, 11768–11781.
- (35) Chang, S. Y.; Davidson, E. R.; Vincow, G. J. *Chem. Phys.* **1968**, *49*, 529–540.
- (36) Chang, S. Y.; Davidson, E. R.; Vincow, G. J. *Chem. Phys.* **1970**, *52*, 5596–5606.
- (37) Vincow, G.; Chang, S. Y.; Davidson, E. R. J. *Chem. Phys.* **1971**, *54*, 4121–4123.
- (38) Vincow, G. J. *Phys. Chem.* **1971**, *75*, 3400–3410.
- (39) Konishi, H.; Morokuma, K. J. *Am. Chem. Soc.* **1972**, *94*, 5603–5612.
- (40) Ellinger, Y.; Subra, R.; Berthier, G. J. *Am. Chem. Soc.* **1978**, *100*, 4961–4963.
- (41) Feller, D.; Davidson, E. R. J. *Chem. Phys.* **1984**, *80*, 1006–1017.
- (42) Fernandez, B.; Jørgensen, P.; Byberg, J.; Olsen, J.; Helgaker, T.; Jensen, H. J. A. J. *Chem. Phys.* **1992**, *97*, 3412–3419.
- (43) Perera, S. A.; Watts, J. D.; Bartlett, R. J. J. *Chem. Phys.* **1994**, *100*, 1425–1434.
- (44) Ohta, K.; Nakatsuji, H.; Hirao, K.; Yonezawa, T. J. *Chem. Phys.* **1980**, *73*, 1770–1776.
- (45) Nakatsuji, H.; Ohta, K.; Yonezawa, T. J. *Phys. Chem.* **1983**, *87*, 3068–3074.
- (46) Engels, B. *Theor. Chem. Acc.* **1993**, *86*, 429–437.
- (47) Salter, E. A.; Trucks, G. W.; Bartlett, R. J. J. *Chem. Phys.* **1989**, *90*, 1752–1766.
- (48) Coulthard, M. A. *Proc. Phys. Soc.* **1967**, *90*, 615–617.
- (49) Quiney, H. M.; Belanzoni, P. *Chem. Phys. Lett.* **2002**, *353*, 253–258.
- (50) Dzuba, V. A.; Flambaum, V. V.; Sushkov, O. P. J. *Phys. B.* **1984**, *17*, 1953–1968.
- (51) Das, T. P. *Hyperfine Interact.* **1987**, *34*, 149–165.
- (52) Das, M.; Chaudhuri, R. K.; Chattopadhyay, S.; Mahapatra, U. S. *Phys. Rev. A* **2011**, *84*, 042512–042519.
- (53) Andriessen, J.; Postma, H.; van den Brink, A. M.; Das, T. P. *Phys. Rev. A* **1992**, *45*, 1389–1398.
- (54) Yuan, X.; Dougherty, R. W.; Das, T. P.; Andriessen, J. *Phys. Rev. A* **1995**, *52*, 3563–3571.
- (55) Filatov, M.; Zou, W.; Cremer, D. J. *Phys. Chem. A* **2012**, *116*, 3481–3486.
- (56) van Wüllen, C. Relativistic Density Functional Theory. In *Relativistic Methods for Chemists*; Barysz, M.; Ishikawa, Y., Eds.; Springer: Dordrecht, 2010; Vol. 10, pp 191–214.
- (57) Engel, E.; Keller, S.; Dreizler, R. M. *Phys. Rev. A* **1996**, *53*, 1367–1374.
- (58) Mayer, M.; Häberlen, O. D.; Rösch, N. *Phys. Rev. A* **1996**, *54*, 4775–4782.
- (59) Geurts, P. J. M.; Bouten, P. C. P.; van der Avoird, A. J. *Chem. Phys.* **1980**, *73*, 1306–1312.
- (60) Eriksson, L. A.; Malkin, V. G.; Malkina, O. L.; Salahub, D. R. J. *Chem. Phys.* **1993**, *99*, 9756–9763.
- (61) Eriksson, L. A.; Malkin, V. G.; Malkina, O. L.; Salahub, D. R. *Int. J. Quantum Chem.* **1994**, *52*, 879–901.
- (62) Ishii, N.; Shimizu, T. *Chem. Phys. Lett.* **1994**, *225*, 462–466.
- (63) Eriksson, L. A.; Malkina, O. L.; Malkin, V. G.; Salahub, D. R. J. *Chem. Phys.* **1994**, *100*, 5066–5075.
- (64) Neese, F. J. *Chem. Phys.* **2003**, *118*, 3939–3948.
- (65) Malkin, I.; Malkina, O. L.; Malkin, V. G.; Kaupp, M. *Chem. Phys. Lett.* **2004**, *396*, 268–276.
- (66) Aquino, F.; Pritchard, B.; Autschbach, J. J. *Chem. Theory Comput.* **2012**, *8*, 598–609.
- (67) van Lenthe, E.; van der Avoird, A.; Wormer, P. E. S. J. *Chem. Phys.* **1998**, *108*, 4783–4796.
- (68) Malkin, E.; Repisky, M.; Komorovsky, S.; Mach, P.; Malkina, O. L.; Malkin, V. G. J. *Chem. Phys.* **2011**, *134*, 044111–044111–8.
- (69) Verma, P.; Autschbach, J. J. *Chem. Theory Comput.* **2013**, *9*, 1052–1067.
- (70) Hrobarik, P.; Repisky, M.; Komorovsky, S.; Hrobarikova, V.; Kaupp, M. *Theor. Chem. Acc.* **2011**, *129*, 715–725.
- (71) Autschbach, J.; Pritchard, B. *Theor. Chem. Acc.* **2011**, *129*, 453–466.
- (72) Valiev, M.; Bylaska, E. J.; Govind, N.; Kowalski, K.; Straatsma, T. P.; Dam, H. J. J. V.; Wang, D.; Nieplocha, J.; Apra, E.; Windus, T. L.; de Jong, W. A. *Comput. Phys. Commun.* **2010**, *181*, 1477–1489.
- (73) van Wüllen, C. J. *Chem. Phys.* **2009**, *130*, 194109–14.
- (74) Schmitt, S.; Jost, P.; van Wüllen, C. J. *Chem. Phys.* **2011**, *134*, 194113–11.
- (75) Aquino, F.; Govind, N.; Autschbach, J. J. *Chem. Theory Comput.* **2011**, *7*, 3278–3292.
- (76) Nichols, P.; Govind, N.; Bylaska, E. J.; de Jong, W. A. J. *Chem. Theory Comput.* **2009**, *5*, 491–499.
- (77) Autschbach, J.; Patchkovskii, S.; Pritchard, B. J. *Chem. Theory Comput.* **2011**, *7*, 2175–2188.
- (78) Autschbach, J.; Ziegler, T. J. *Chem. Phys.* **2000**, *113*, 936–947.
- (79) Visscher, L.; Dyall, K. *At. Data Nucl. Data Tables* **1997**, *67*, 207–224.
- (80) Andrae, D. *Phys. Rep.* **2000**, *336*, 413–527.
- (81) Autschbach, J. *ChemPhysChem* **2009**, *10*, 2274–2283.
- (82) van Lenthe, E.; Wormer, P. E. S.; van der Avoird, A. J. *Chem. Phys.* **1997**, *107*, 2488–2498.
- (83) van Wüllen, C. *Mariapfarr 2012 workshop lecture notes, Part 3*; <http://www.uni-graz.at/tchwww/mariapfarr12/vanWuellen.zip> (accessed Dec. 2012).
- (84) Bylaska, E. J.; de Jong, W. A.; Govind, N.; Kowalski, K.; Straatsma, T. P.; Valiev, M.; van Dam, J. J.; Wang, D.; Apra, E.; Windus, T. L.; Hammond, J.; Autschbach, J.; Aquino, F.; Nichols, P.; Hirata, S.; Hackler, M. T.; Zhao, Y.; Fan, P.-D.; Harrison, R. J.; Dupuis, M.; Smith, D. M. A.; Glaesemann, K.; Nieplocha, J.; Tipparaju, V.; Krishnan, M.; Vazquez-Mayagoitia, A.; Jensen, L.; Swart, M.; Wu, Q.; Van Voorhis, T.; Auer, A. A.; Nooijen, M.; Crosby, L. D.; Brown, E.; Cisneros, G.; Fann, G. I.; Fruchtl, H.; Garza, J.; Hirao, K.; Kendall, R.; Nichols, J. A.; Tsemekhman, K.; Wolinski, K.; Anchell, J.; Bernholdt, D.; Borowski, P.; Clark, T.; Clerc, D.; Dachsel, H.; Deegan, M.; Dyall,

- K.; Elwood, D.; Glendening, E.; Gutowski, M.; Hess, A.; Jaffe, J.; Johnson, B.; Ju, J.; Kobayashi, R.; Kutteh, R.; Lin, Z.; Littlefield, R.; Long, X.; Meng, B.; Nakajima, T.; Niu, S.; Pollack, L.; Rosing, M.; Sandrone, G.; Stave, M.; Taylor, H.; Thomas, G.; van Lenthe, J.; Wong, A.; Zhang, Z. *NWChem, A Computational Chemistry Package for Parallel Computers, Version 6 (2012 developer's version)*; Pacific Northwest National Laboratory: Richland, WA, 2011.
- (85) Kutzelnigg, W.; Fleischer, U.; Schindler, M. The IGLO-Method: Ab Initio Calculation and Interpretation of NMR Chemical Shifts and Magnetic Susceptibilities. In *NMR Basic Principles and Progress*; Diehl, P.; Fluck, E.; Gunther, H.; Kosfeld, R.; Seelig, J., Eds.; Springer-Verlag: Heidelberg, Germany, 1990; Vol. 23, pp 165–262.
- (86) Roos, B. O.; Lindh, R.; Malmqvist, P.; Veryazov, V.; Widmark, P. *J. Phys. Chem. A* **2005**, *109*, 6575–6579.
- (87) Roos, B. O.; Lindh, R.; Malmqvist, P. A.; Veryazov, V.; Widmark, P.-O. *Chem. Phys. Lett.* **2005**, *409*, 295–299.
- (88) Becke, A. D. *Phys. Rev. A* **1988**, *38*, 3098–3100.
- (89) Perdew, J. P. *Phys. Rev. B* **1986**, *33*, 8822–8824.
- (90) Perdew, J. P.; Burke, K.; Ernzerhof, M. *Phys. Rev. Lett.* **1997**, *78*, 1396–1396.
- (91) Adamo, C.; Barone, V. *J. Chem. Phys.* **1999**, *110*, 6158–6170.
- (92) Yanai, T.; Tew, D. P.; Handy, N. C. *Chem. Phys. Lett.* **2004**, *393*, 51–57.
- (93) Nakajima, T.; Hirao, J. *J. Chem. Phys.* **2002**, *116*, 8270–8275.
- (94) Tsuchiya, T.; Abe, M.; Nakajima, T.; Hirao, K. *J. Chem. Phys.* **2001**, *115*, 4463–4472.
- (95) Baerends, E. J.; Ziegler, T.; Autschbach, J.; Bashford, D.; Bérces, A.; Bickelhaupt, F. M.; Bo, C.; Boerrigter, P. M.; Cavallo, L.; Chong, D. P.; Deng, L.; Dickson, R. M.; Ellis, D. E.; van Faassen, M.; Fan, L.; Fischer, T. H.; Fonseca Guerra, C.; Ghysels, A.; Giammona, A.; van Gisbergen, S. J. A.; Götz, A. W.; Groeneveld, J. A.; Gritsenko, O. V.; Grüning, M.; Gusarov, S.; Harris, F. E.; van den Hoek, P.; Jacob, C. R.; Jacobsen, H.; Jensen, L.; Kaminski, J. W.; van Kessel, G.; Kootstra, F.; Kovalenko, A.; Krykunov, M. V.; van Lenthe, E.; McCormack, D. A.; Michalak, A.; Mitoraj, M.; Neugebauer, J.; Nicu, V. P.; Noodleman, L.; Osinga, V. P.; Patchkovskii, S.; Philipsen, P. H. T.; Post, D.; Pye, C. C.; Ravenek, W.; Rodríguez, J. I.; Ros, P.; Schipper, P. R. T.; Schreckenbach, G.; Seldenthuis, J. S.; Seth, M.; Snijders, J. G.; Solà, M.; Swart, M.; Swerhone, D.; te Velde, G.; Vernooijs, P.; Versluis, L.; Visscher, L.; Visser, O.; Wang, F.; Wesolowski, T. A.; van Wezenbeek, E. M.; Wiesenekker, G.; Wolff, S. K.; Woo, T. K.; Yakovlev, A. L. *Amsterdam Density Functional, SCM, Theoretical Chemistry*; Vrije Universiteit: Amsterdam, The Netherlands, 2008. Available online: <http://www.scm.com>.
- (96) Notter, F.-P.; Bolvin, H. *J. Chem. Phys.* **2009**, *130*, 184310.
- (97) Baldas, J.; Boas, J. F.; Bonnyman, J.; Williams, G. A. *J. Chem. Soc., Dalton Trans.* **1984**, 2395–2400.
- (98) Liese, W.; Dehnicke, K.; Rogers, R. D.; Shakir, R.; Atwood, J. L. *J. Chem. Soc., Dalton Trans.* **1981**, 1061–1063.
- (99) Cohen, A. J.; Mori-Sánchez, P.; Yang, W. *Science* **2008**, *321*, 792–794.
- (100) Henderson, T. M.; Scuseria, G. E. *Mol. Phys.* **2010**, *108*, 2511–2517.
- (101) Polo, V.; Gräfenstein, J.; Kraka, E.; Cremer, D. *Chem. Phys. Lett.* **2002**, *352*, 469–478.
- (102) van Lenthe, E.; van der Avoird, A.; Hagen, W. R.; Reiijerse, E. J. *J. Phys. Chem. A* **2000**, *104*, 2070–2077.
- (103) Stein, M.; van Lenthe, E.; Baerends, E. J.; Lubitz, W. *J. Phys. Chem. A* **2001**, *105*, 416–425.
- (104) Stein, T.; Autschbach, J.; Govind, N.; Kronik, L.; Baer, R. *J. Phys. Chem. Lett.* **2012**, 3740–3744.
- (105) Verma, P.; Perera, A.; Bartlett, R. J. *Chem. Phys. Lett.* **2012**, *524*, 10–15.
- (106) Verma, P.; Bartlett, R. J. *J. Chem. Phys.* **2012**, *136*, 044105.
- (107) Verma, P.; Bartlett, R. J. *J. Chem. Phys.* **2012**, *137*, 134102.
- (108) Malkin, I.; Malkina, O. L.; Malkin, V. G.; Kaupp, M. *J. Chem. Phys.* **2005**, *123*, 244103–16.
- (109) Perdew, J. P.; Ruzsinszky, A.; Constantin, L. A.; Sun, J.; Csonka, G. I. *J. Chem. Theory Comput.* **2009**, *5*, 902–908.
- (110) Knight, L. B., Jr.; Fisher, T. A.; Wise, M. B. *J. Chem. Phys.* **1981**, *74*, 6009–6013.
- (111) De Vore, T. C.; Weltner, W. *J. Am. Chem. Soc.* **1977**, *99*, 4700–4703.
- (112) Kirmse, R.; Köhler, K.; Abram, U.; Böttcher, R.; Golic, L.; De Boer, E. *Chem. Phys.* **1990**, *143*, 75–82.
- (113) Lack, G. M.; Gibson, J. F. *J. Mol. Struct.* **1978**, *46*, 299–306.
- (114) Knight, L. B., Jr.; Weltner, W., Jr. *J. Chem. Phys.* **1971**, *55*, 2061–2070.
- (115) Lon B. Knight, J.; Lin, K. C. *J. Chem. Phys.* **1972**, *56*, 6044–6049.
- (116) Kasai, P. H.; McLeod, D. *J. Phys. Chem.* **1978**, *82*, 1554–1559.
- (117) Knecht, S.; Fux, S.; Meer, R.; Visscher, L.; Reiher, M.; Saue, T. *Theor. Chem. Acc.* **2011**, *129*, 631–650.
- (118) Butler, J. E.; Hutchison, C. A., Jr. *J. Chem. Phys.* **1981**, *74*, 3102–3119.
- (119) Case, D. A. *J. Chem. Phys.* **1985**, *83*, 5792–5796.